REVIEW ARTICLE

3D/4D Ultrasound in Gynecology

Ashok Khurana

Consultant in Reproductive Ultrasound, The Ultrasound Lab, Defence Colony, New Delhi, India

Correspondence: Ashok Khurana, Consultant in Reproductive Ultrasound, The Ultrasound Lab, C 584, Defence Colony, New Delhi 110024, India, e-mail: ashokkhurana@ashokkhurana.com

Abstract

Three-dimensional (3D) and real-time three-dimensional (4D) technology, 3D power Doppler and high frequency transducers are being increasingly used in gynecological ultrasound. This treatise discusses practical aspects of these techniques and audits the utility and advantages of these indications in guiding and improving patient outcomes. Current literature places these techniques as a method of choice to image morbid pelvic anatomy and pathophysiology.

Keywords: 3D/4D, ultrasound in gynecology, 3D power Doppler, three-dimensional imaging, ultrasound morphology, ultrasound techniques.

The impact of newer and dramatic technologies is always under scrutiny and it is prudent to periodically reassess the utility of these methods in the perspective of improving patient outcomes. An audit of this nature also needs to be done in the perspective of cost-effectiveness, cost containment, and health priorities, since the cost of health is ultimately to be borne by each member of a community or nation, irrespective of whether the health provider is reimbursed by the state, by an insurance arrangement or directly by a patient.

This paper discusses the state of the art and science of 3D and 4D ultrasound techniques in gynecology.

TECHNOLOGICAL ADVANCES

Two technical advances have greatly influenced the widespread use of ultrasound in gynecological disease in the last decade. These include variable and high frequency transvaginal transducers and the utilization of 3D power Doppler technology.

Higher transducer frequencies improve resolution. The trade-off is, however, decreased depth of penetration. Newer transducers combine frequencies as high as 12 MHz with a multifrequency option of low (about 5 MHz) and mid frequency, thereby allowing combinations of high resolution and depth penetration by using keys and knobs on the console. Increased 2D resolution implies sharper and more accurate images in 3D and 4D as well.

The second technological advance is the combination of power Doppler with 3D. About a decade and a half ago reports appeared of a newer Doppler technique now widely called power Doppler. Unlike conventional color Doppler, where flow information represents flow direction, mean velocity and range of velocities, power Doppler is a technique that assesses amplitude or energy. Information displayed represents reflected (scatter) information from clumps of red blood cells within the sampled vessel. The greater the clump density, the higher the amplitude of the signal and, therefore, the brighter the color coding. The technique is known by several names, including power Doppler, power angiography, color Doppler energy, color amplitude imaging and amplitude-mode color Doppler ultrasound. Mathematically speaking, the signal represents the area under the power spectral curve. The technique, by its very nature, enhances low flow sensitivity and this makes it an excellent method for detecting slow flow vessels and areas of omnidirectional vessels. A gain of 10 to 15 dB is achieved without interference by noise. This method of detecting flow information has consequently emerged as the method of choice for studying parenchymal flow in normal and pathological areas in the pelvis. Although, the information display lacks direction information, directional information can be obtained from any image by a spectral Doppler waveform study. As power Doppler is less angle dependent, tortuous vessels are more completely demonstrated.

DATA ACQUISITION AND DISPLAY

Automated devices to acquire volume data for 3D evaluation have largely replaced freehand devices. In the freehand method the transducer was manually moved through the region of interest and a position sensor registered the slice in space and time, or alternatively, image based software was built into the 3D package. The freehand method could be used on-line where the ultrasound unit managed all

functions, or, off-line where the analog video output was fed into a workstation. The transducer and attachments in the free-hand system were bulky and awkward to use particularly in the vagina. Most units currently in use, therefore, are automated 3D probes. These are unit specific, more accurate and easy to use. When these units are employed, an area of interest is chosen in the real time 2D image and the size and depth are outlined. A speed of acquisition is then selected and the acquisition activated. The transducer elements automatically sweep through the volume box chosen. It is pertinent to note that the slower the speed of acquisition, the higher the resolution. Resolution is highest in the plane of acquisition. Additionally, the closer the plane of acquisition to the plane of study the better the resolution. The machine automatically receives and stores data from the region of interest and displays it in an orthogonal format (Figs 1A to D). Images may then be rendered by various algorithms, which rely on the difference between acoustic impedances at tissue interfaces and have been variably named by various manufacturers.

In conventional ultrasound, the uterus is visualized as a variably thick, linear or ovoid structure in longitudinal, transverse and oblique plane. The shape of the cavity is difficult to assess, as is the coronal plane. With 3D, the entire extent of the endometrium and myometrium can be shown, including the corpus, fundus, cervix and cornual areas. Coronal, sagittal and transverse planes can be simultaneously displayed to permit more exhaustive viewing (Figs 2A to C). The images may be automatically zoomed in or out (Fig. 3). Once acquired, the volume data can be reviewed by first rotating the planes to obtain standard anatomic orientations and then scrolling through the entire data to locate and characterize lesions, both focal and diffuse. Multiplanar orthogonal viewing offers virtually unlimited numbers of planes, and time constraints should not impede the endeavor to obtain information. In fact, the additional time spent on a 3D gynecologic scan is far less than on 3D obstetric scan because this time is spent not so much on data acquisition but in exploring the data obtained. The time factor would, of course, depend on the complexity of a case and on operator expertise. In experienced hands the exercise takes no more than three to ten minutes. Once identified in any one plane, the lesion can be marked by a center point, and this center point is automatically displayed in all three

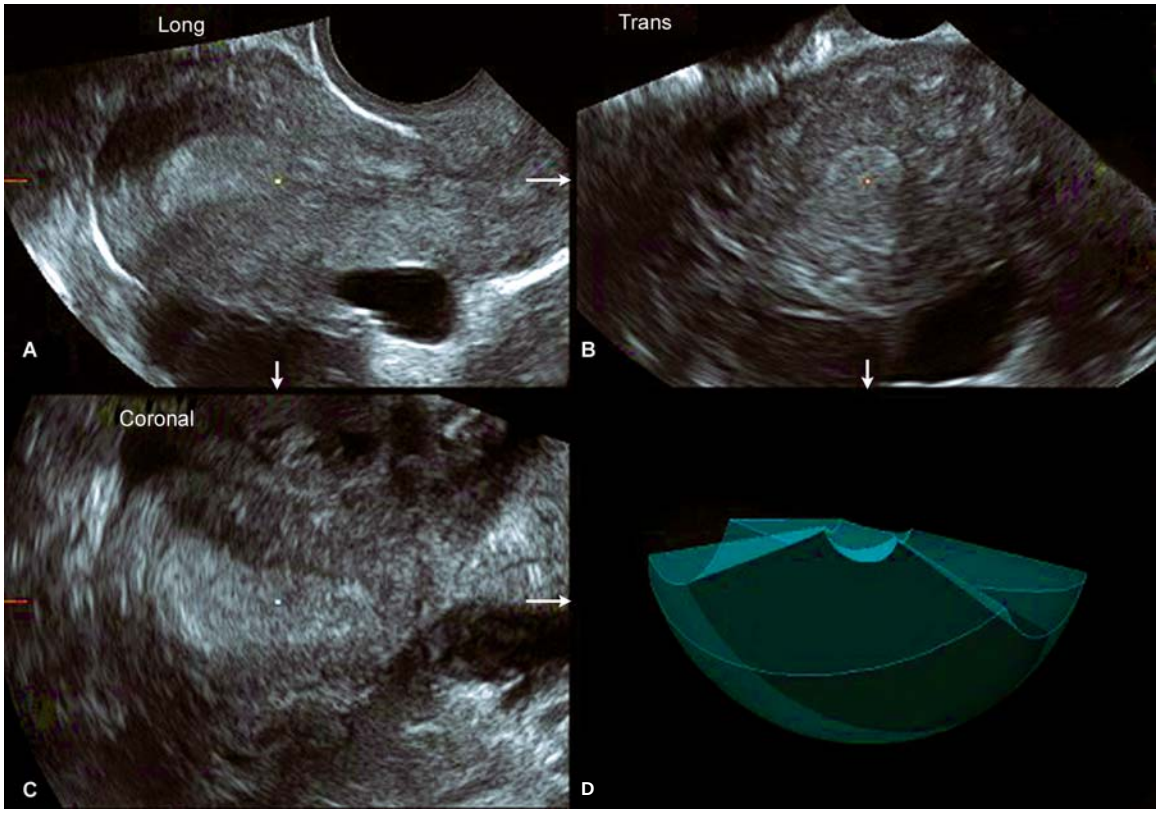

Figs 1A to D: 3D units sweep through the region of interest and store the entire information in computer memory. Knobs on the keyboard are employed to reconstruct any desired plane. One of the most useful and commonly employed display formats is the display in three orthogonal planes: longitudinal, transverse and coronal. The coronal view is difficult to obtain on 2D scans and remarkably easy to visualize with 3D

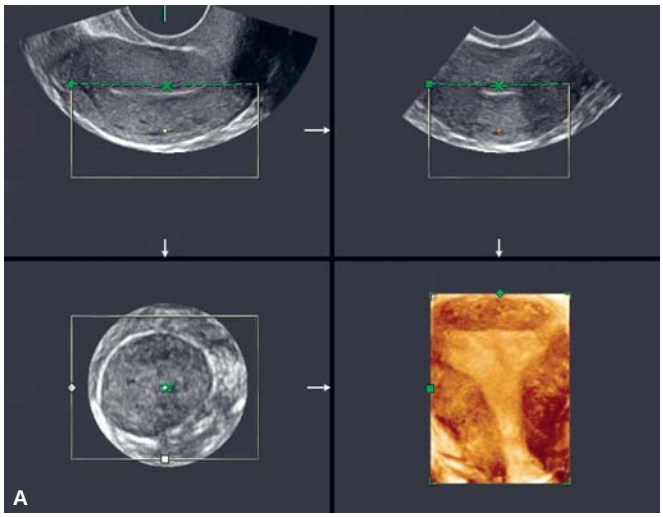

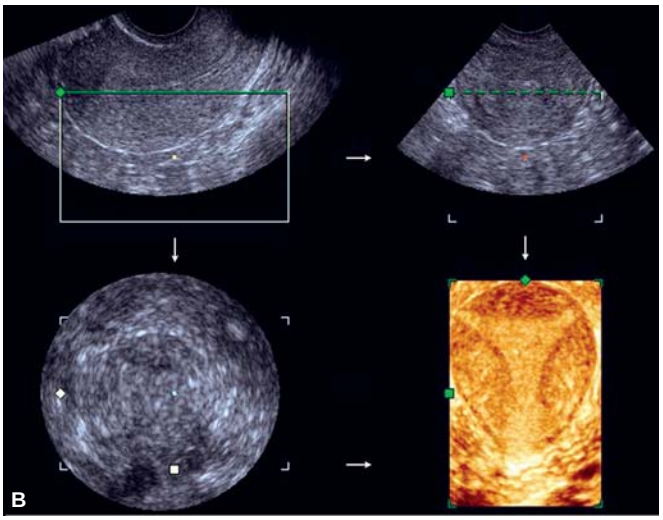

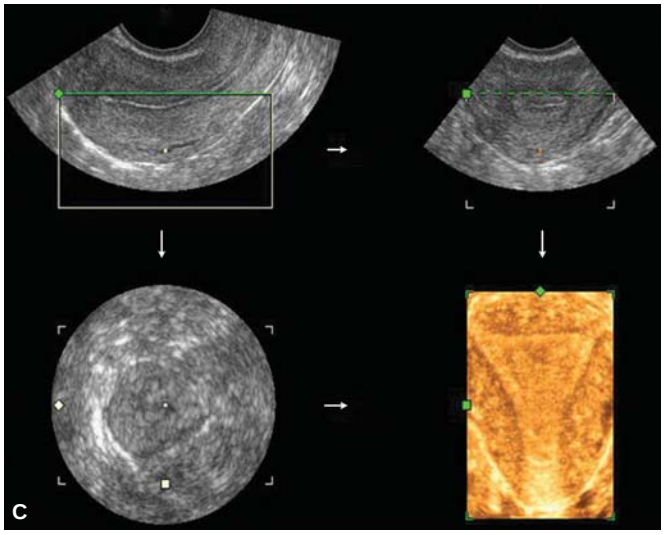

Figs 2A to C: (A and B) 3D rendered displays show the entire configuration of the cavity including the tubal ostia, corpus and cervix. Note the convex contour of the uterine cavity and the subtle concavity of the fundal aspect of the cavity. These features exclude any uterine duality or septations. The hypoechoic zone around the cavity is a normal feature and is important to delineate because it loses definition in adenomyosis, endometritis and neoplastic conditions. All three rendered images show a normal uterus. Note how the triangular configuration can differ within the normal population. Rendered images can be obtained even in a thin endometrium, (C) While rotating orthogonal planes to render the endometrium in the region of the ostia, the cavity may show hypoechoic artifacts (<<) which represents areas of myometrium. This can be confirmed by referring to the orientation of the plane of interest in the selected plane of imaging (the longitudinal selected plane in this case) and should not be mistaken for focal endometrial lesions

orthogonal planes. All or part of the studied volume can be automatically rendered and displayed as a single image or along with the orthogonal planes. The evaluation can be enhanced by using volume measurements, niche mode studies (Fig. 4), power Doppler studies (Fig. 5), translational cine studies (Figs 6A to D) or a retrospective review of stored data. Unlike obstetric 3D, surface rendering is infrequently required in gynecologic 3D studies except in saline infusion sonohysterography, where it often adds diagnostic information. The entire acquired data can be transmitted electronically to obtain second opinions, facilitate remote conferencing with experts, and, can be efficiently stored for review and recall.

The sagittal plane is selected for volume measurements and the other two planes for ensuring that the entire pathology is included in the measured area. Surface rendering permits contoural evaluation. Niche mode and translational cine studies permit a virtual tour of the entire

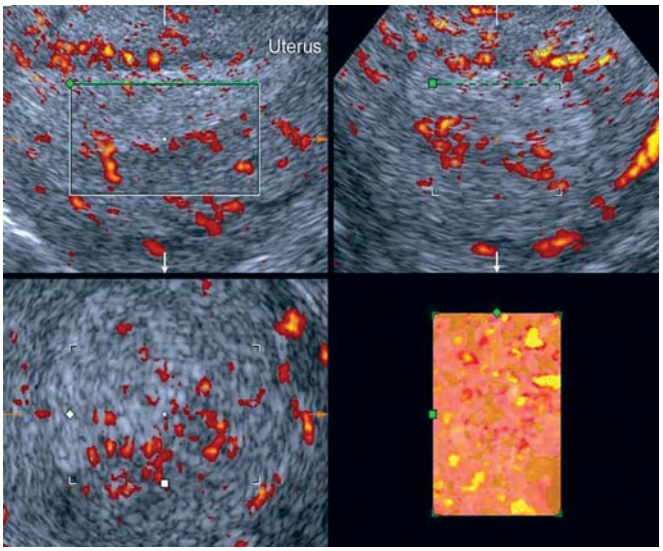

Fig. 3: 3D acquisition can be obtained simultaneously in grey scale and color Doppler/power Doppler modes. These may be zoomed in for better visualization

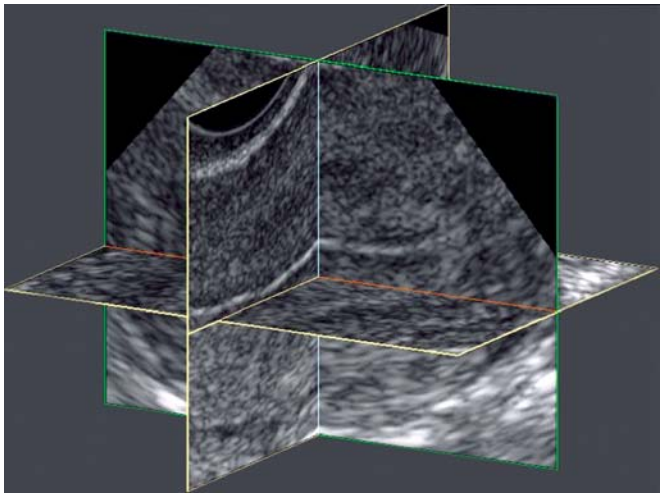

Fig. 4: Niche mode studies permit a biplanar scrolling through acquired data. These are useful for enhancing accuracy of identifying and localizing lesions

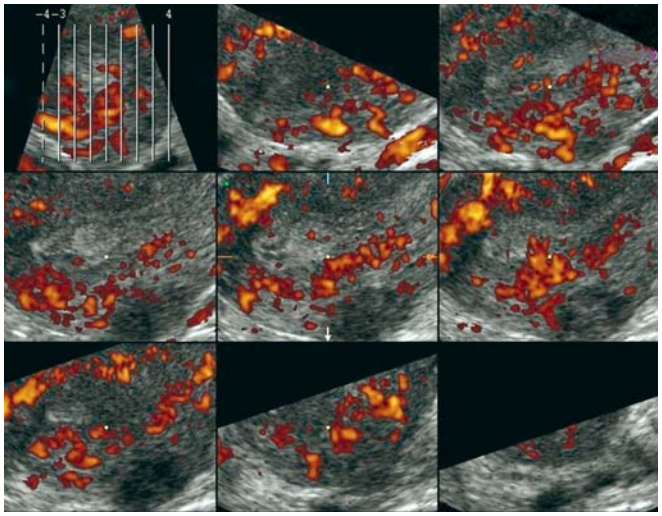

Fig. 5: Grey scale and power Doppler 3D acquisitions may be displayed in a tomographic sectional format akin to CT and MR. This format permits excellent localization and identification of pathological lesions and vascular signals

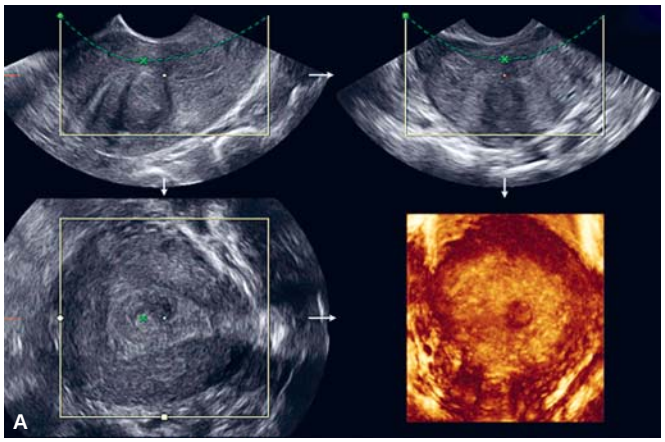

Fig. 6A

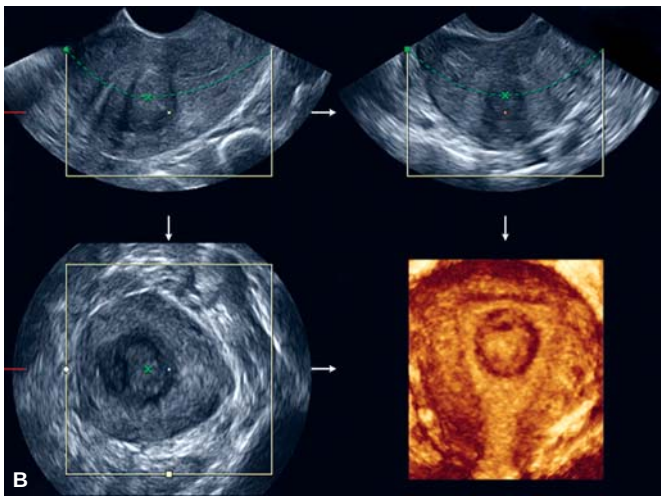

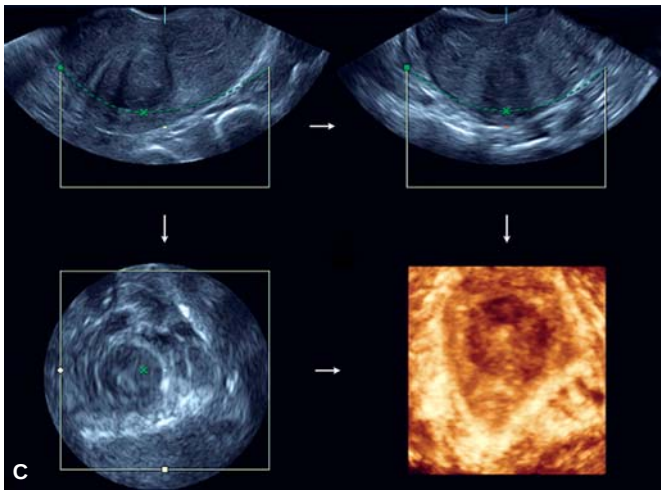

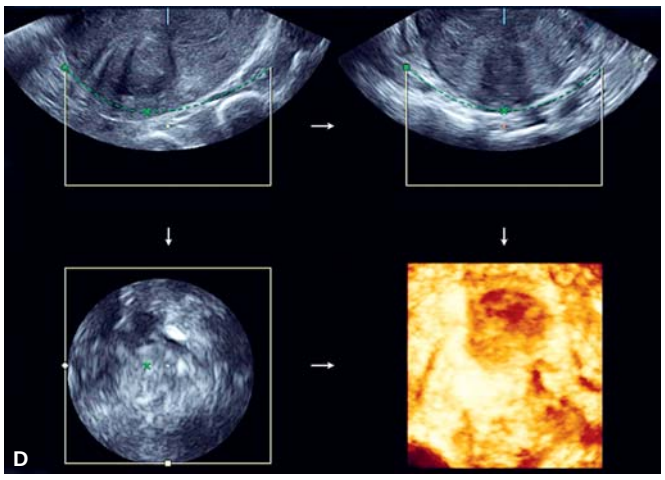

Figs 6A to D: Translation cine scrolls automatically through a chosen volume of interest yielding cine sections through the block. Figures A to D show stills from a translation cine sequence from the anterior to the posterior aspect of a uterus with a posterior wall fibroid. Careful translational studies reveal that this fibroid extends from the cavity to the surface and is not just interstitial as would be presumed from the 2D and 3D rendered images

lesion and surrounding tissue along including an evaluation of vascular morphology where necessary, by a manual and automatic mode respectively. 3D power Doppler permits an unsurpassed view of vascularity and permits quantification of neovascularization. 3D saline infusion sonohysterography enhances the sensitivity in select situations. 4D studies are useful in saline infusion sonohysterography for storing data sets, excluding the need for reinstillation, permitting multiplanar analysis and allowing magnification of stored data during re-evaluation.

In patients who have not been sexually active, 3D data acquisition via the rectum, using an intracavitary transducer, can greatly enhance delineation of pelvic lesions and developmental abnormalities when compared to transabdominal 3D studies.

3D data is basically a sum total of 2D data sets, and, as a logical consequence, a 3D study does not replace a 2D study. It, in fact, extends the wealth of information obtainable from an ultrasound scan.

MULLERIAN ANOMALIES

Anomalous Mullerian development is estimated to occur in 3 to 4% of women[1] and about half of these are associated with clinical disease.[2-4] The clinical significance lies in the associated infertility, implantation failures,[5] miscarriages,[6] premature labor, malpresentations, uterine irritability, fetal growth and dystocia.[4,7] Correction of these anomalies by hysteroscopy and other minimally invasive surgical procedures greatly improves reproductive outcomes.[8,9] Precise delineation of the type and extent of the anomaly is important to assess the need for surgical correction and the technique of correction.[6,9-11]

2D transvaginal scanning is a sensitive screening tool[12,13] for developmental uterine malformations but lacks specificity and is markedly operator dependent.[14,15] Often a minimal and usually clinically innocuous duality, such as an arcuate uterus, may display two endometrial stripes in an axial section through the fundus.[16] This results in a false positive diagnosis with embarassing situations at operative hysterocopy! The markers for uterine duality in conventional ultrasound include a double endometrial echo complex, a wide transverse uterine diameter, and rarely, a distinctive complete uterine duality.[17] For several decades, X-ray contrast hysterosalpingography has been the technique for evaluation of uterine malformations. Although, the technique is reasonably safe, it involves radiation exposure and lacks specificity in detailing lateral fusion anomalies.[18] The outline of the cavity can be displayed in accurate detail. However, and understandably, the surface contour of the uterus cannot be evaluated. Since the differentiation of a septate from a bicornuate uterus is based on the morphology of the fundal contour and not the morphology of the cavity, hysterosalpingography is an inadequate method for complete delineation. For some years now, saline infusion sonohysterography has evolved as an adjunct to transvaginal 2D sonography.[15,17,19] The procedure, however, fails to differentiate the septate uterus from the bicornuate uterus because the surface contour of the uterus and fundus cannot be delineated by this technique either. In fact, a hysteroscopy alone also fails to make this distinction and a concurrent laparoscopy needs to be carried out to make a complete diagnosis. This is important because the repair is so distinctively different in the two diagnoses. Magnetic resonance imaging (MRI) can delineate these malformations since it images the cavity and the fundal surface contour. The method is, however, expensive and the software is cumbersome and coarse.[20,21] 3D ultrasound with its inherent ability to demonstrate the entire endometrium and the myometrium is emerging as a sensitive and remarkably specific modality for mapping the anomalous uterus.[12,22,23] It is becoming increasingly apparent that precise anatomical information can be obtained without the need for radiation, contrast material or surgical intervention.[18,16]

The unique ability of 3D ultrasound to display the coronal plane and the immense possibilities of multiplanar display consequent to interactive manipulation of acquired data sets, has placed this modality as the optimal method for evaluating the structurally anomalous uterus.

Similar to the technique used to evaluate the uterus for acquired pathologic processes, the method for obtaining 3D data remains the transvaginal automated, dedicated transducer. These are unit specific and more accurate and easy to use. The data obtained by these units is easy to manipulate and has far fewer artifacts especially for the relatively uninitiated observer. The 3D window should include the entire uterine contour seen on an appropriately zoomed in 2D image. The transducer elements automatically sweep through the volume box chosen. For enhanced resolution, a slow sweep speed and a longitudinal sweep are selected. In patients who have not been sexually active, data may be obtained by a transrectal scan. Once acquired, the data can be reviewed, stored, retrieved, brainstormed, transmitted by phone lines or satellite and networked. It is imperative to obtain one 3D data set in the power Doppler mode in order to display a vascular guidemap to the congenitally malformed uterus as this has a bearing on management protocols[24-26] (Figs 7A and B). In a uterine duality where the horns have a largely horizontal orientation, an additional acquisition in the coronal plane may be useful. Very rarely, in such uteri, it may not be possible to obtain

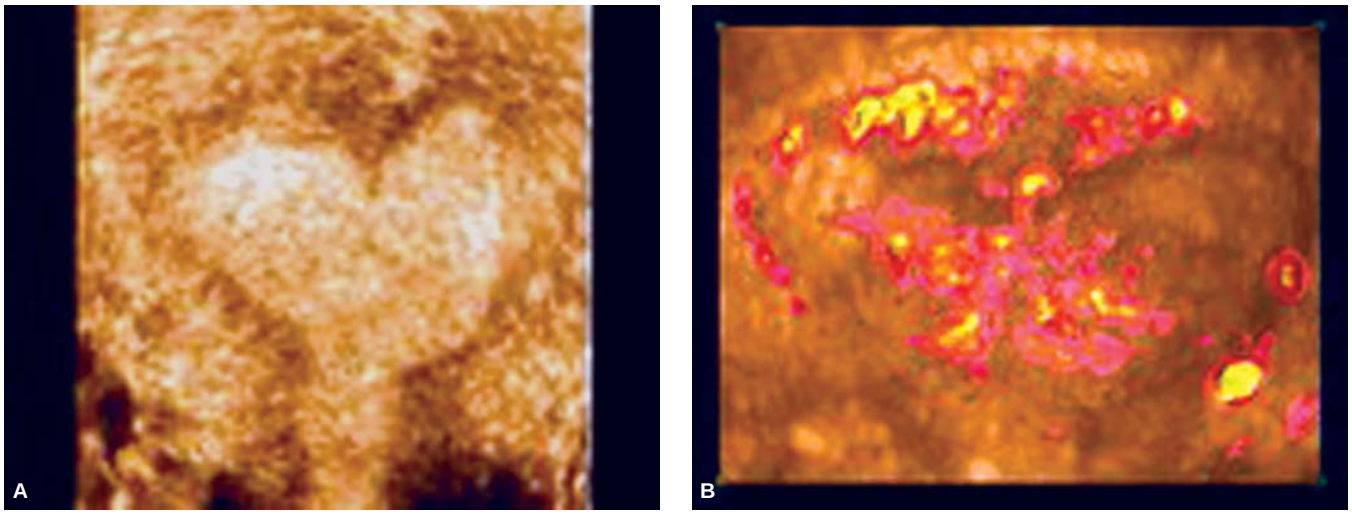

Figs 7A and B: (A) 3D rendering of a subseptate uterus, (B) 3D power Doppler rendering reveals an extensively vascular septum. This is associated with a poor prognosis

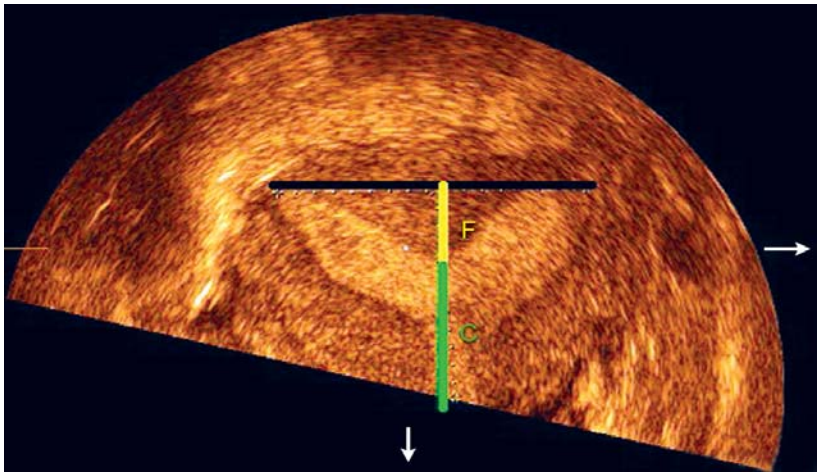

Fig. 8: Mullerian anomalies can be quantified. A horizontal line is drawn between the two ostia. F represents distance of the depth of the septum from this line. C represents the vertical extent of the residual cavity and has a bearing on prognosis

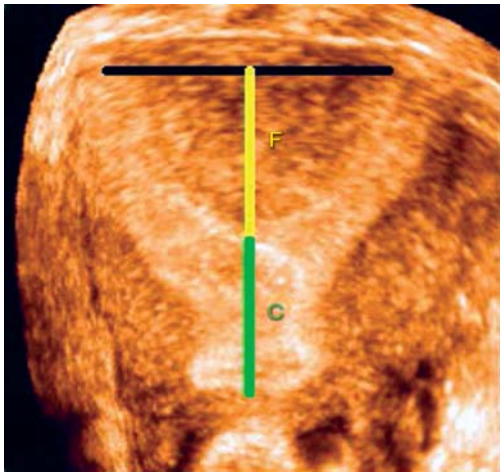

Fig. 9: 3D rendered coronal image of a subseptate uterus. The length of the septum is considerably longer than the length of the residual cavity and indicates relatively poor prognosis

both horns and the entire cervix in a single rendered image. Surface rendering may be required in some cases to assess the fundal contour.[22] 3D acquisition of Saline Infusion Sonohysterography yields excellent details of global uterine anatomy. However, it is being realized that the superb contrast resolution of 3D techniques is rapidly reducing the yield of these studies in evaluating Mullerian anomalies. In the presence of concurrent uterine pathology such as fibroids and polyps in the anomalous uterus, however, 3D sonohysterography is a useful problem solving modality.[27] Positive contrast sonohysterography was described for better cavity delineation in the past but currently is rarely employed.[28] Quantification of developmental uterine anomalies is possible[29] (Fig. 8). The tubal ostia are delineated in the coronal plane and a line drawn through them. The midpoint of this line is extended to the inferiormost point of indentation of the uterine cavity or the extent of the septum (distance F). The other measurement taken is the vertical extent of the uterine cavity (distance C). These distances are reliably reproducible[30] and the ratio F/F+C can be obtained. In women who have recurrent pregnancy losses, the length of the indentation or the length of the septum are not as important. It is the vertical height of the residual uterine cavity, which is considerably shorter, and the degree of distortion that is considerably greater, in women with recurrent pregnancy losses (Fig. 9).

Paired Mullerian ducts appear in the embryo at six weeks of gestation. Soon thereafter, these fuse in the midline in their caudal extent. This is known as lateral fusion. A septum representing the fused segments gradually breaks down, resulting in one uterine cavity. The fused portions form the uterus, cervix and upper two thirds of the vagina. The cranial

portions of the Mullerian ducts remain unfused and form the fallopian tubes. Developmental malformations are consequent to truncation of normal development, abnormal fusion or disordered resorption.[1] Failure of development of both Mullerian ducts results in agenesis of the uterus or in a hypoplastic uterus. Unilateral failure results in a unicornuate uterus. Failure of lateral fusion results in a didelphys uterus or a bicornuate uterus. Failure of resorption of the septum results in a septate or arcuate uterus.

The nomenclature of developmental anomalies of the uterus remained confusing for several years. The American Fertility Society[10] (AFS) Classification Scheme based on embryological derangements, has put these in an appropriate perspective and facilitates a precise diagnosis, which can then be managed by proven protocols that improve obstetric outcomes.

AFS Class I includes uterine agenesis and hypoplasia. 3D studies are useful for calculating uterine size and assessing canalization. Class II is a unicornuate uterus. A true unicornuate uterus is the result of complete unilateral arrest of Mullerian development. If the arrest of development is partial, as is more usual, a rudimentary horn with or without functioning endometrium is present. 2D ultrasound is frequently unable to identify the subtle findings of a unicornuate uterus. 3D rendered images reveal a banana shaped relatively narrow uterus with or without a rudimentary horn (Figs 10A and B). Multiplanar imaging helps to confirm a single cornual angle.[16] Class III refers to a didelphys uterus, which is a result of complete nonfusion of the Mullerian ducts. The two horns are usually fully developed and two cervices are present (Figs 11 to 12B). There may be an associated transverse vaginal septum

Fig. 11: 3D rendered coronal image of a uterus didelphys. The two horns and two cervices are clearly evident

(Figs 13A to D). All these features can be evaluated with ease and accuracy with 3D techniques. The cervices are very close to each other but the canals are distinct. Class IV is a bicornuate uterus. This results from partial nonfusion of the Mullerian ducts. The central myometrium may extend to the internal os (bicornuate unicollis) (Figs 14A and B) or the external os (bicornuate bicollis) (Fig. 15). The horns are typically low normal or small in size. A 3D orthogonal plane study with coronal reformatting is the method of choice for evaluating these uteri. A midsagittal indentation of 10 mm or more is evident in the bicornuate uterus (Fig. 16). Class V is a septate uterus. This results from a failure of resorption of the septum between the fused Mullerian ducts. The septum may be shallow (subseptate) (Fig. 17) or extensive (down to the external os) (Fig. 18), fibrous,

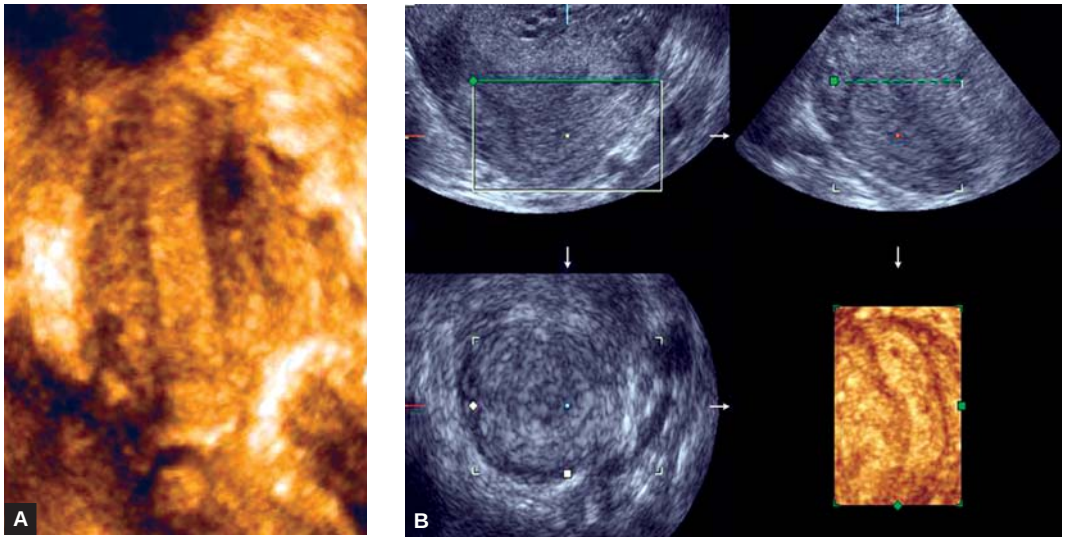

Figs 10A and B: Elongated narrow uterus with no cornual angle: unicornuate uterus

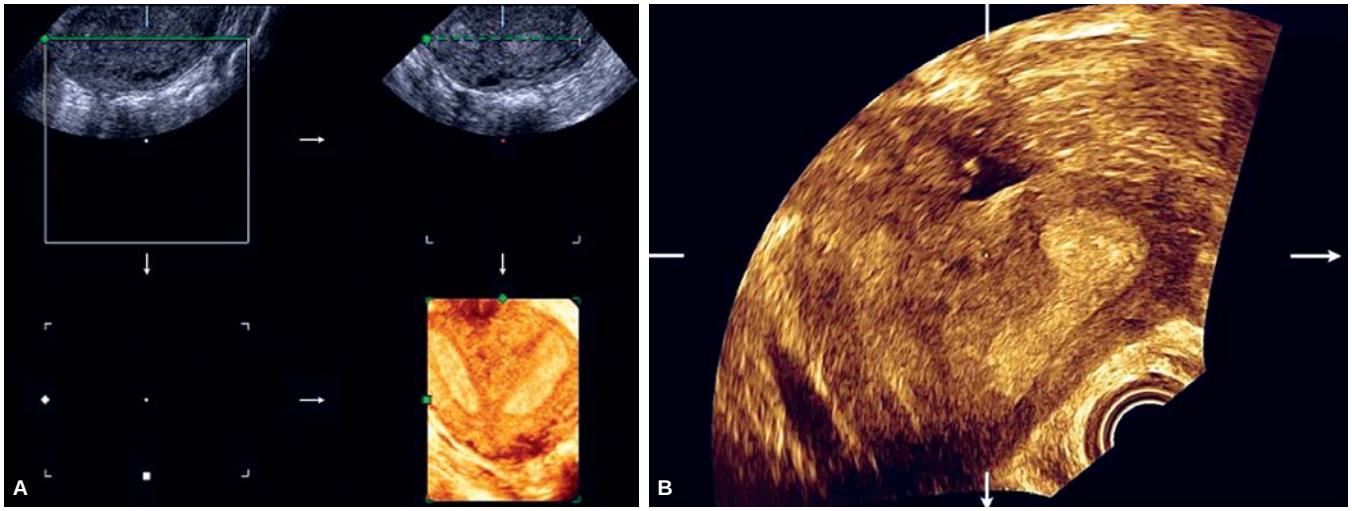

Figs 12A and B: Uterus didelphys. The uterine cavity is well-defined on either side. The cervices were poorly defined even on 3D scans. Examination under anesthesia and cervical dilatation confirmed a narrow spiral cervix on either side

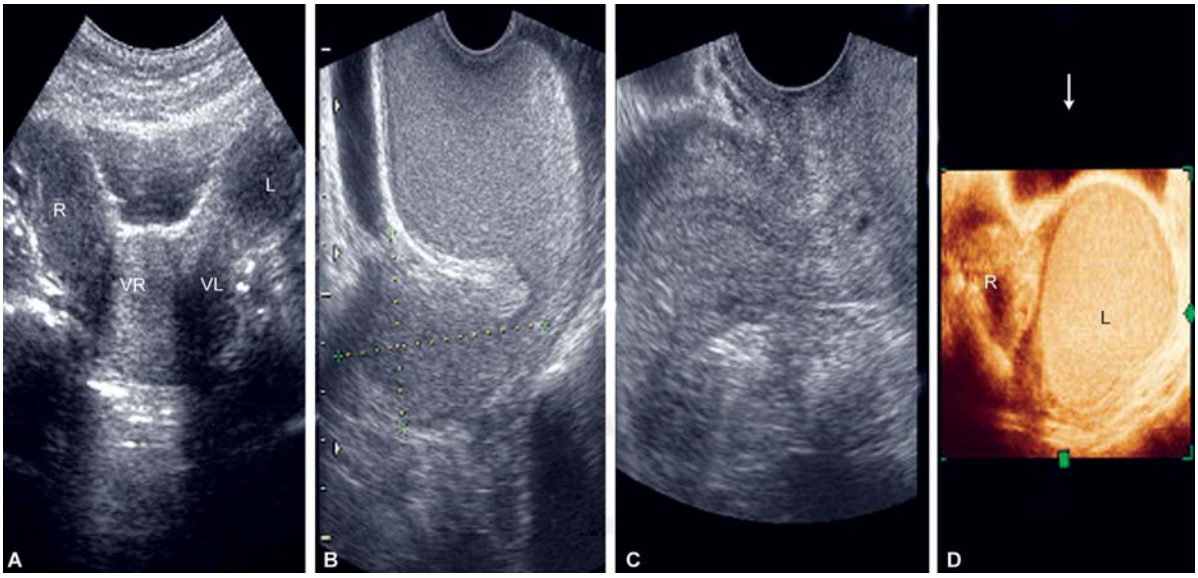

Figs 13A to D: Evaluation of a patient of primary amenorrhea who has never been sexually active. The transabdominal scan reveals a didelphys uterus with possibly two vaginas (A). There is a right hematocolpos seen on a transrectal scan (B). This also reveals a normal left horn, cervix and vagina (C). 3D rendering confirms a dual vagina with a right hematocolpos (D)

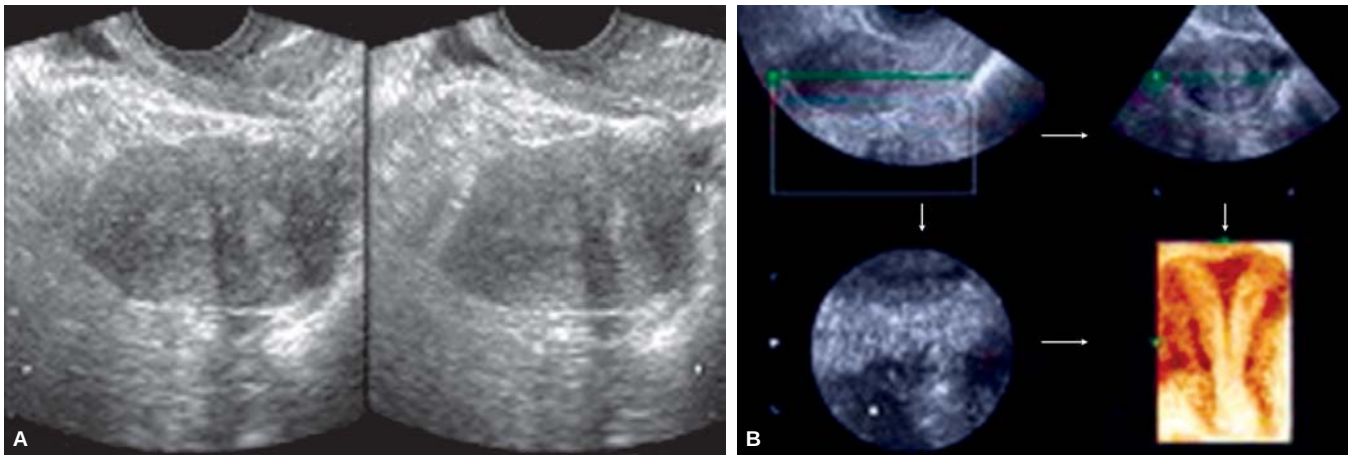

Figs 14A and B: (A) 2D transvaginal scan showing two uterine cavities. (B) 3D coronal rendering reveals a bicornuate uterus with a single cervix

Fig. 15: 3D rendered image of a bicornuate uterus with two cervices

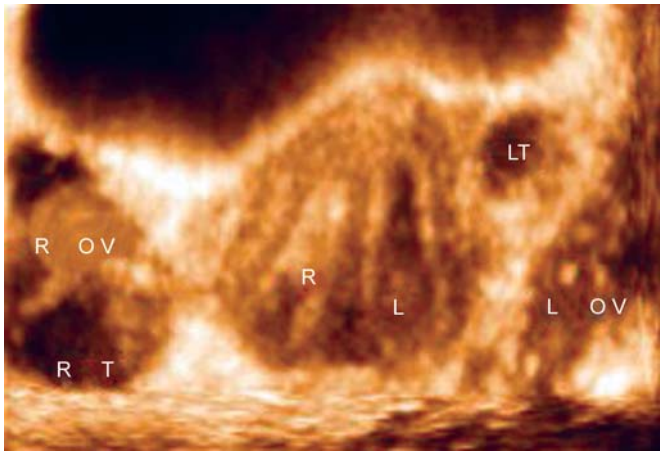

Fig. 16: 3D rendered image of a bicornuate uterus with a bilateral hematometra and bilateral hydrosalpinx

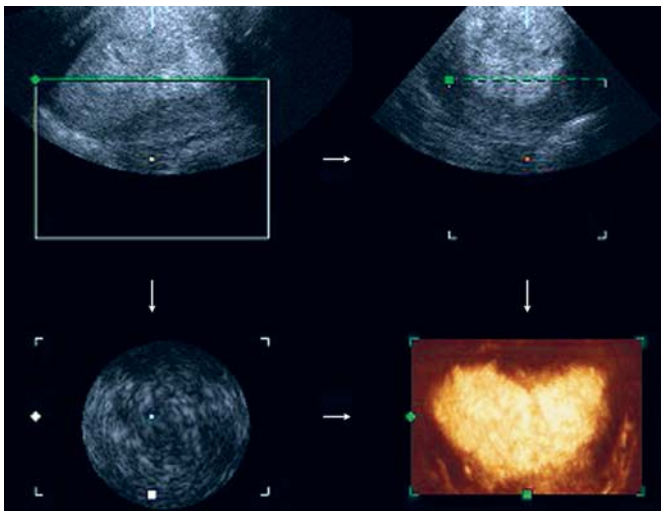

Fig. 17: 3D rendered image in the coronal plane revealing a shallow fundal muscular septum and a longer fibrous septum

muscular or mixed. The septate uterus may be associated with a septate cervix, a septate vagina or both. Coronal plane analysis is necessary for assessing this condition and differentiating it from a bicornuate uterus. Recognition of this condition is imperative because obstetric outcomes greatly improve with hysteroscopic metroplasty in appropriately selected cases. With bicornuate and didelphys uteri, the approach has to be an abdominal one. In recent years, 3D criteria have helped greatly in patient selection.[26,29] The muscular septum lacks supporting connective tissue,[25] and shows poor preovulatory changes and poor decidualisation with consequently poor placentation. Additionally, a vascular septum shows enhanced irritability.[31] Most septa show poor vascularization responses in the pregnant state. Although, the incidence of septate uteri is similar in patients with recurrent pregnancy losses compared to women with normal obstetric outcomes, there is no doubt that the height of the residual uterine cavity and the degree of distortion are related to poor outcomes. The degree of indentation and the height of the septum do not correlate with poor outcomes. It has been traditional obstetric practice not to treat a subseptate uterus until two pregnancy losses have occurred. Poor obstetric outcomes and the accurate information obtained by 3D now justify septal resection by a hysteroscopic method as soon as they are diagnosed.

The arcuate uterus comes in class VI of the AFS classification. The cavity is single but demonstrates a convexity towards the cavity. This is less than 10 mm in height from an imaginary line between the cornua. The serous contour of the fundus is convex or flat. The arcuate uterus is rarely associated with pregnancy failures. The pathophysiology for poor reproductive outcomes in these uteri is not known. Hysteroscopic fundal repair does not improve outcomes and the only treatment suggested is a cervical cerclage to prevent premature labor and delivery. Class VII of the classification refers to the T-shaped uterine cavity (Fig. 19) of the type seen in children of mothers who have been on diethylstilboestrol. The T-shaped uterus has now been observed in some patients who have had no intrauterine exposure to diethylstilboestrol. Patients are likely to benefit from a hysteroscopic lateral metroplasty.

FOCAL ENDOMETRIAL LESIONS

Although 2D studies can identify a large number of focal lesions in the endometrium, saline infusion sonohysterography (SISH) enhances the sensitivity of identifying polyps. 3D techniques with their inherent increased contrast resolution have reduced the need for sonohysterography. Saline infusion sonohysterography can be combined with

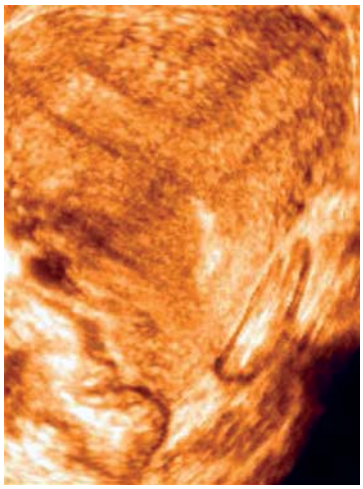

Fig. 18: 3D rendered image showing a subseptate uterus with an extensive separation of the two horns

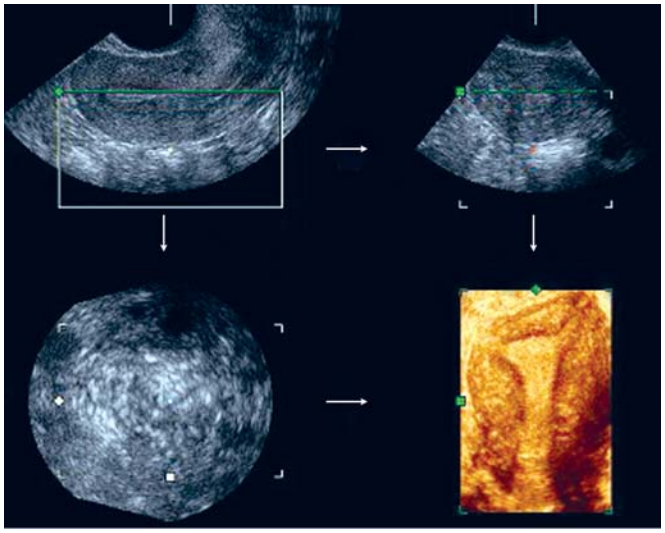

Fig. 19: 3D rendered image of a T-shaped uterus. The vertical limb of the cavity is remarkably long

3D to increase the sensitivity of both techniques.[27,32] 3D also increases the possibility of identifying multiple polyps and multiple endometrial lesions (Figs 20A and B). Power Doppler studies are useful to assess the origin and vascular pattern of polyps.[32] 3D Power Doppler can help differentiate fibroid polyps from endometrial polyps and adenomyomatous polyps. Endometrial polyps typically show a solitary feeding vessel (Figs 21A to D). Fibroid polyps often show only peripheral flow (Fig. 22). Central flow in fibroid polyps is secondary to degeneration, inflammation and very rarely consequent to a sarcomatous change. Adenomyomatous polyps show a typical spoke-wheel appearance with a central large vessel and radiating smaller vessels (Figs 23A to C). Quantific indices such as peak systolic velocity, diastolic velocity, systolic diastolic ratios, Resistive Index, Pulsatility Index, Time to peak velocity and 3D vascular indices are not reliable predictors of the histopathology of these focal endometrial lesions.

Malignant endometrial lesions in the endometrium are difficult to characterize when they are small. Larger lesions are poorly marginated, variably vascular and when invasive, obscure the endometrial-myometrial interface. Focal increased echogenecity, diffuse increased echogenecity and diffuse inhomogeneity on 2D studies increase the predictability of pathologic findings.[33-40] In addition, these findings, even in an endometrium which is thinner that the cutoff values of normal postmenopausal endometrium, are indicators for inclusion in the group for invasive endometrial sampling. Aggressive evaluation for a malignancy must be made if there is a focal increased echogenecity or a diffuse inhomogeneity even in a thin endometrium.[41] 3D endometrial volume, although initially promosing,[32] is no longer regarded as a significant solitary parameter for discerning

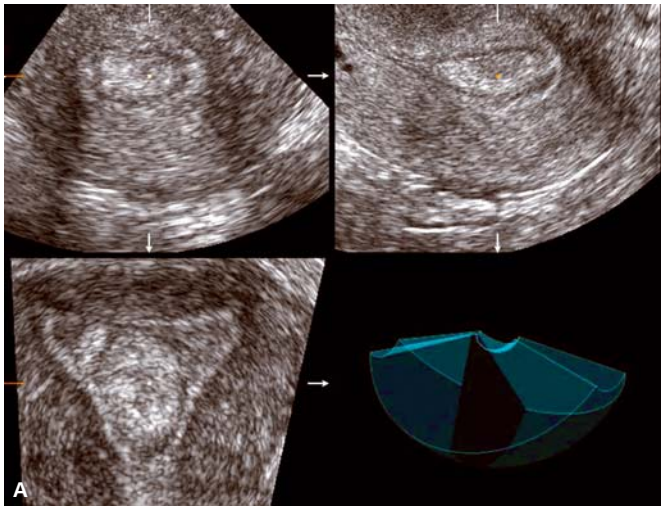

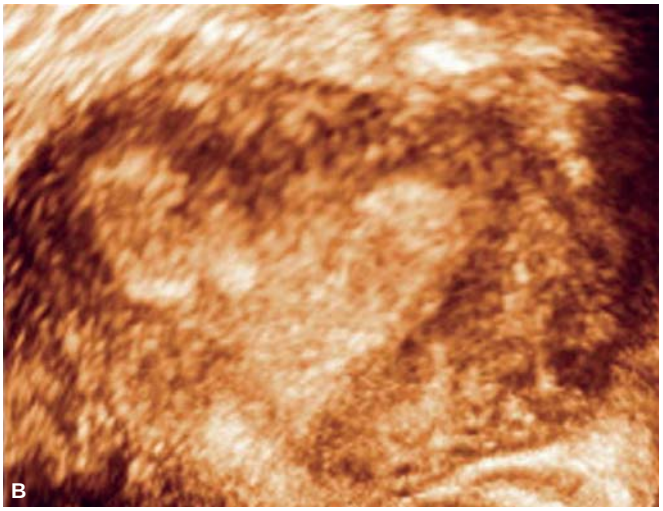

Figs 20A and B: (A) 3D orthogonal displays help to identify multiplicity of polyps, (B) When lesions in the endometrium are concurrent such as polyps, congenital uterine malformations and fibroids, the ultrasound image may be dramatic or confused. MR is useful in such situations. This 3D rendering shows a subseptate uterus with submucous fibroids and polyps

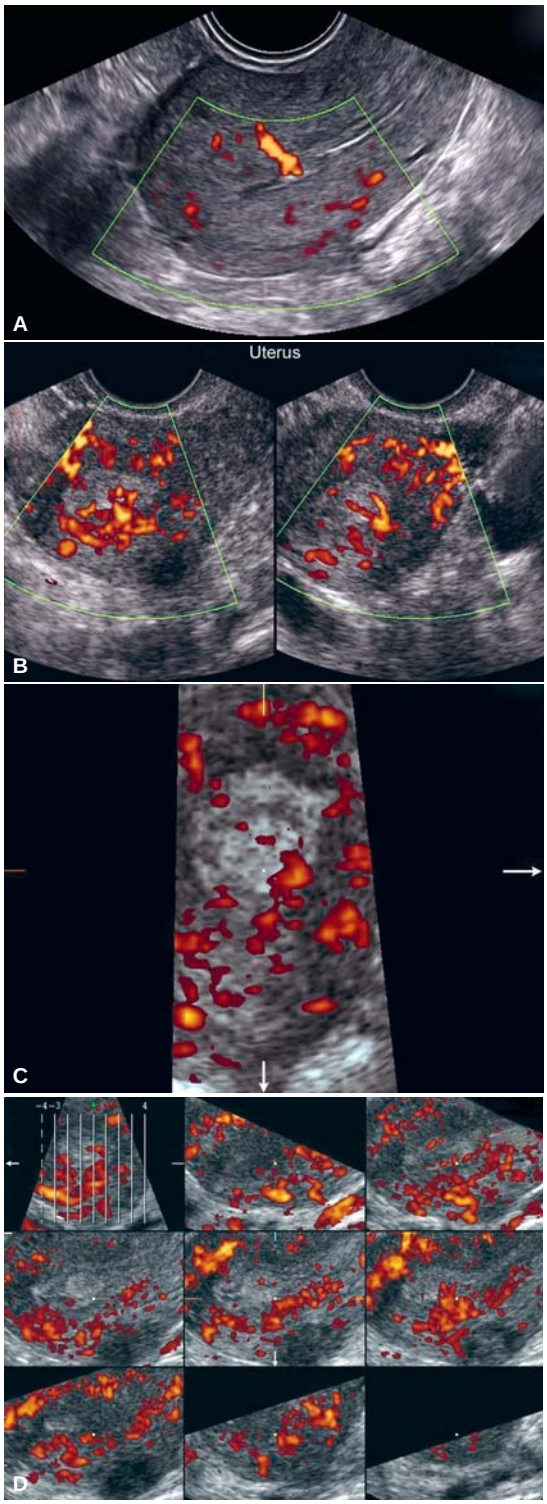

Figs 21A to D: (A) Endometrial polyps typically show a solitary feeding vessel. This usually shows no branching and becomes smaller and smaller as it reaches the center of the lesion. (B) Dichotomous branching of a feeder vessel should raise a strong suspicion for a malignant histopathology. (C) Coronal reconstructed images are useful to identify feeding vessels, (D) Tomographic ultrasound imaging is a 3D technique that permits sectional imaging in parallel planes. This is useful for identifying the number and location of polyps. Grey scale and power Doppler intensities can be displayed simultaneously

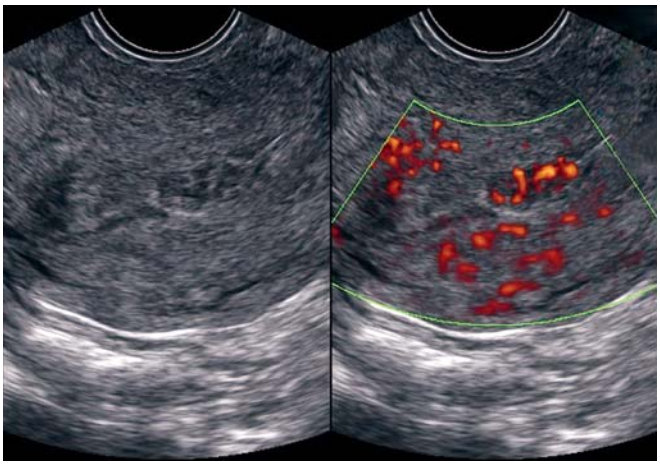

Fig. 22: Fibroid polyps often show only peripheral flow. Central flow secondary to degeneration, inflammation or sarcomatous change may also be evident

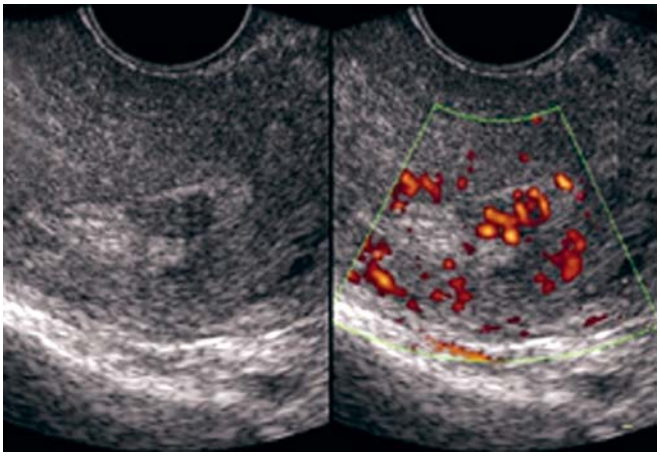

Fig. 23A: Adenomyomatous polyps show a typical spoke-wheel appearance with a central large vessel and radiating smaller vessels

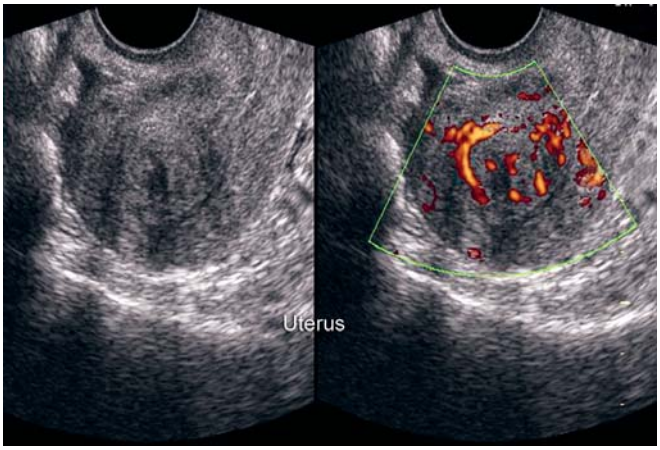

Fig. 23B: Central flow in adenomyomatous polyps of the endometrium may not always have a spoke-wheel appearance. In these situations central vessels are randomly distributed and have no specific pattern

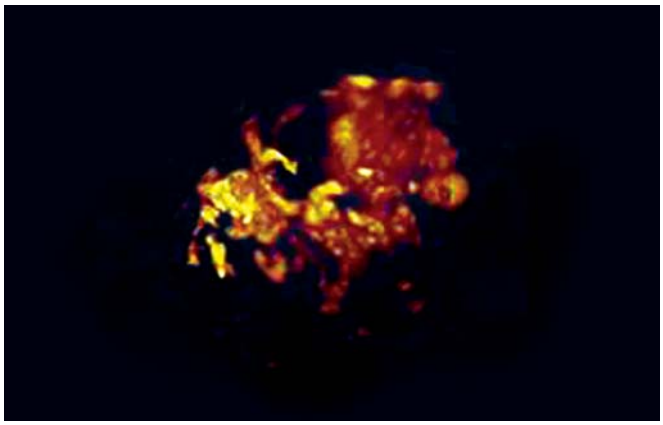

Fig. 23C: In adenomyomatous polyps can sometimes radiate from two areas within the lesions. This is not necessary a sign of a malignant change

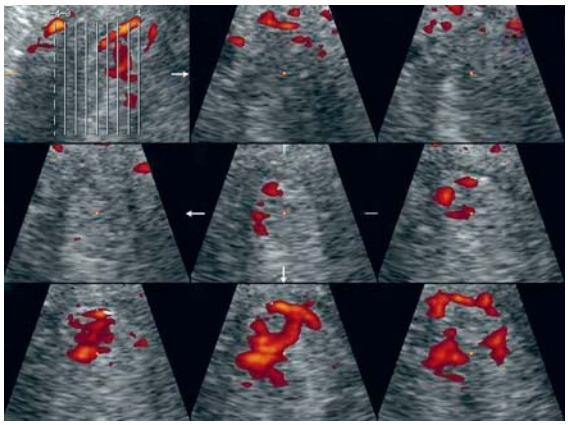

Fig. 24C: Same patient as in figures 24A and 24B showing markedly abnormal caliber vessels when analysed with 3D tomographic ultrasound Imaging studies. Histopathology confirmed a poorly differentiated endometrial carcinoma

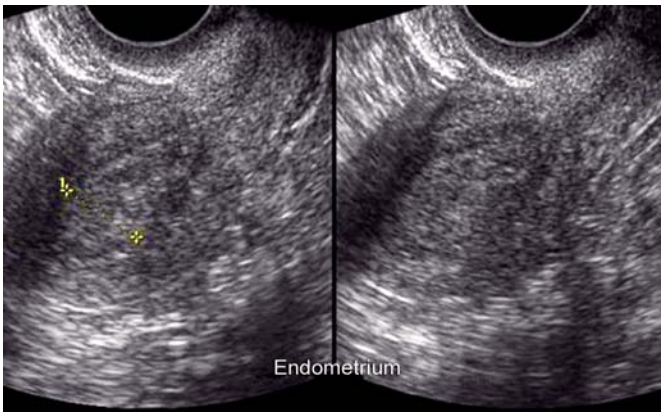

Fig. 24A: 15 mm thick, inhomogeneous endometrium with a poorly differentiated endometrial/myometrial interface of the posterior wall suggesting a strong possibility of an endometrial cancer

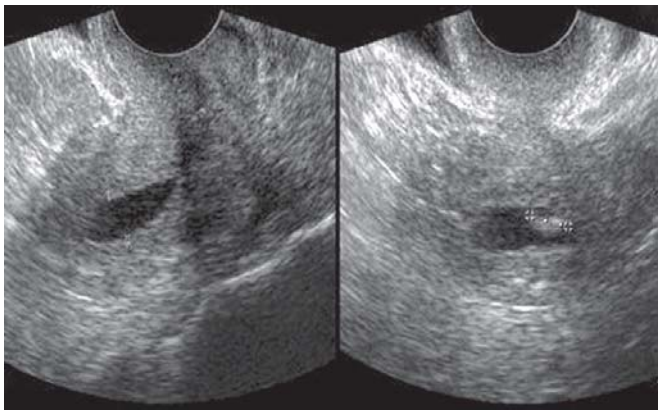

Fig. 25A: Transvaginal scan showing an endometrial fluid collection with echogenic areas within it. It is difficult to differentiate whether this corresponds to debris or a mass

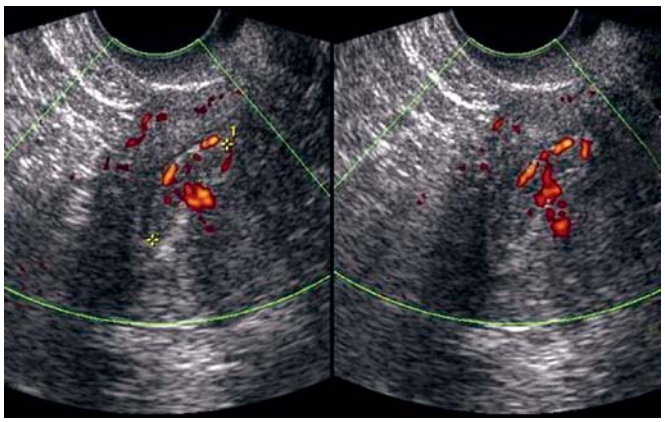

Fig. 24B: Same case as in figure 24A showing dilated and tortuous feeder vessels

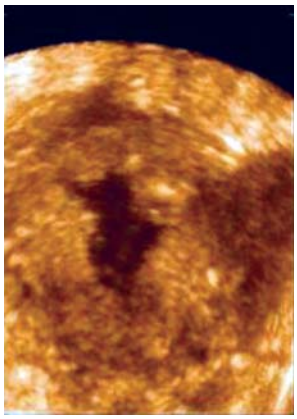

Fig. 25B: 3D rendering of the endometrium in the same patient as figure 25A. Note the thick lobulated endometrium. Hysteroscopy confirmed a malignancy confined to the endometrium

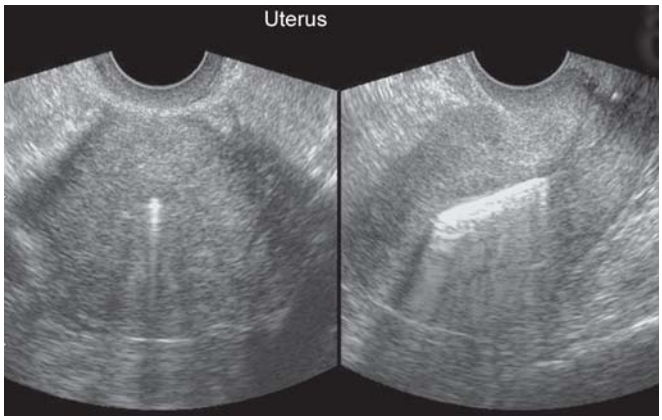

Fig. 26A: Intrauterine device in the uterine cavity in a patient with lost threads. The device is confirmed to lie within the cavity

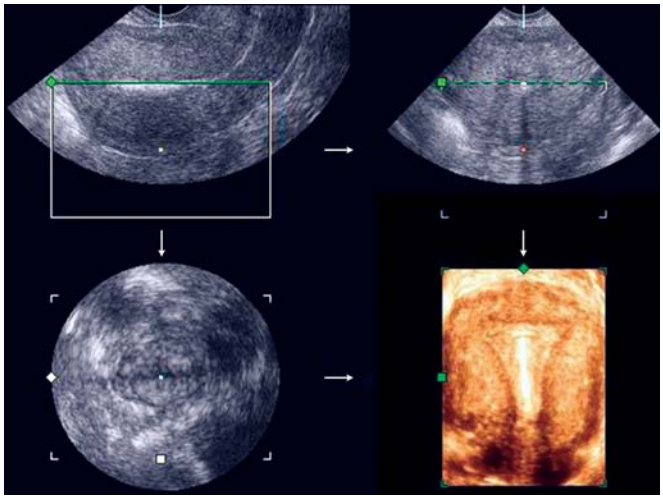

Fig. 26B: 3D reconstruction of the same patient as in figure 26A. 3D confirms the normal location of the device

Fig. 26C: 3D permits recognition of various types of intrauterine devices. This rendering shows a multiload device in the uterine cavity

endometrial malignancy from benign lesions[38,40] and needs to be assessed in the perspective of echo texture and vascularity. 3D power Doppler demonstration of dichotomous branching of a feeder vessel is a strong marker of a malignant mass (Figs 24A to C). Other markers for endometrial malignancy include dilated, saccular, tortuous vessels and arteriovenous anastamoses. The shaggy surface of malignant masses is easier to identify in the presence of endometrial fluid collections with 3D techniques (Figs 25A and B) and with saline infusion sonohysterography.

Intrauterine Devices

These are normally located in the cavity in the fundus and upper part of the uterine corpus. Migration into the myometrium is associated with lost threads, pain and abnormal vaginal bleeding. A low location is associated with a higher rate of contraceptive failure. The type of device can be readily identified only by 3D rendering (Figs 26A to C). This technique also improves delineation of abnormal migration of a device. Medicated devices are often less echogenic than copper loaded devices. It must be remembered that once a device has migrated beyond the myometrium and into the peritoneum or bowel, it is very difficult to identify with ultrasound. In this situation, conventional abdominal X-ray imaging is useful to identify or exclude the presence of the device in the abdomen or pelvis.

Endometrial Fluid Collections

Free fluid collections in the endometrial cavity are physiological in the immediate postmenstrual phase and in menopause. These are thin-walled and clear. Any focal thickening or vascularization of the endometrium associated with free fluid in the cavity warrants histopathological sampling. Echogenecity within fluid contained in the uterine cavity may represent menstrual debris, inflammatory debris, blood or pus. Only a gross examination and microscopy can reveal the pathological basis in these situations. Adhesive bands can be seen as echogenic or trilaminar variably thick structures that traverse the uterine cavity. These are largely missed on routine 2D scans but well delineated with 3D saline infusion sonohysterography (Figs 27A to G). Failure to sharply delineate the endometrial contour should raise the suspicion for adhesive bands. Sensitivity for detecting adhesions is best in the secretory phase of the menstrual cycle.

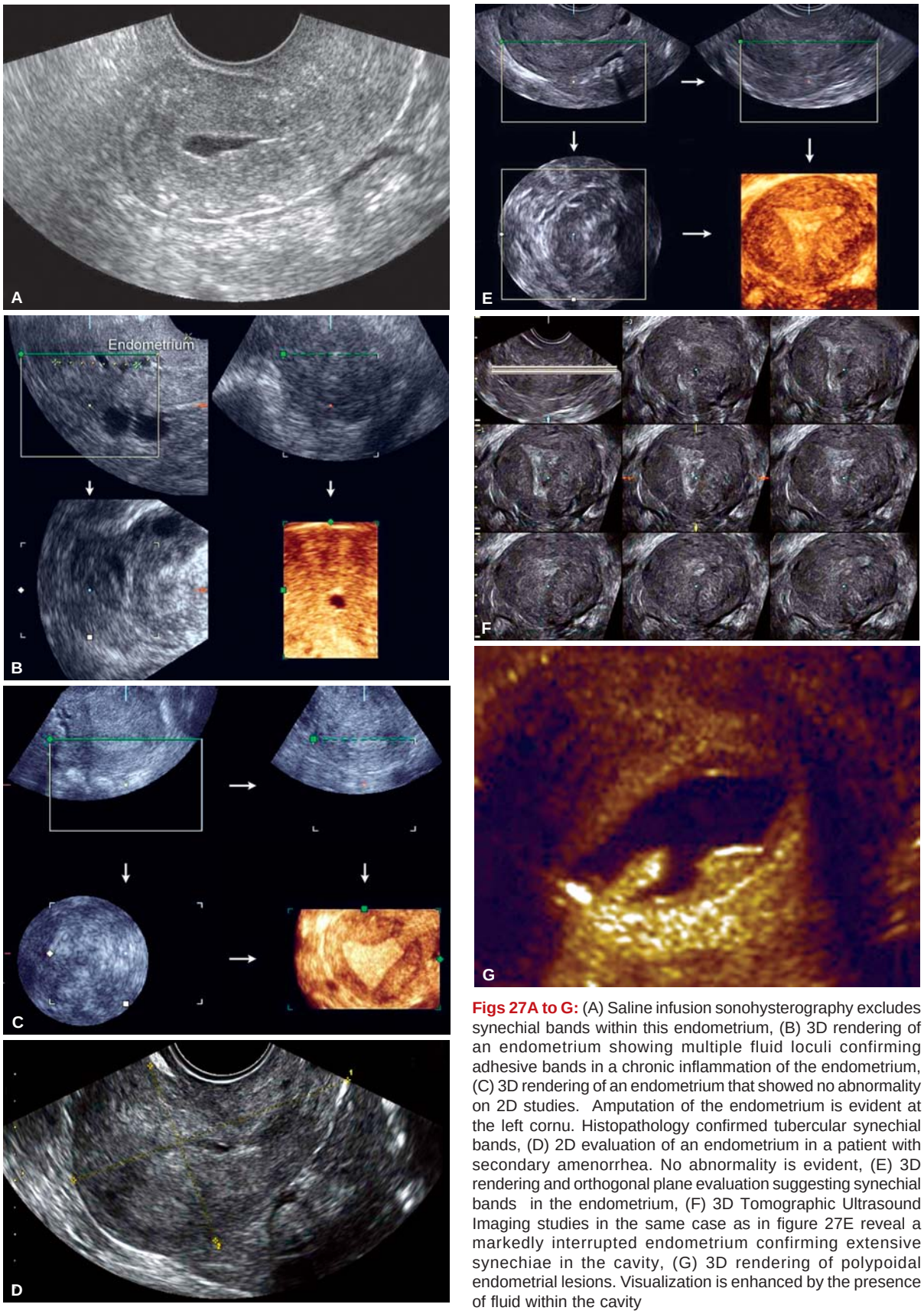

Figs 27A to G: (A) Saline infusion sonohysterography excludes synechial bands within this endometrium, (B) 3D rendering of an endometrium showing multiple fluid loculi confirming adhesive bands in a chronic inflammation of the endometrium, (C) 3D rendering of an endometrium that showed no abnormality on 2D studies. Amputation of the endometrium is evident at the left cornu. Histopathology confirmed tubercular synechial bands, (D) 2D evaluation of an endometrium in a patient with secondary amenorrhea. No abnormality is evident, (E) 3D rendering and orthogonal plane evaluation suggesting synechial bands in the endometrium, (F) 3D Tomographic Ultrasound Imaging studies in the same case as in figure 27E reveal a markedly interrupted endometrium confirming extensive synechiae in the cavity, (G) 3D rendering of polypoidal endometrial lesions. Visualization is enhanced by the presence of fluid within the cavity

Endometrial Receptivity

Currently available ultrasound techniques of evaluation for endometrial receptivity include gray-scale sonography using high frequency transvaginal scans, conventional color Doppler studies, power Doppler, three-dimensional and real-time three-dimensional (4D) studies and Tomographic Ultrasound Imaging.

The parameters that have been studied over the past two decades, moreso the last four years, include endometrial thickness, endometrial volume, endometrial ultrasound morphology, subendometrial peristalsis, endometrial and subendometrial vascularization, subendometrial vascularization, myometrial echogenecity, myometrial power Doppler, spectral analysis of uterine artery flow velocity waveforms and perifollicular vascularization.

Endometrial thickness below 6 to 8 mm is rarely associated with conception.[42-45] Increase in endometrial thickness above this level, however, does not enhance implantation rates and there is no difference in the mean endometrial thickness in patients who become pregnant and those who do not become pregnant in ART cycles.[46] The minimum endometrial volume (Fig. 28) associated with pregnancy is 1.59 ml as calculated by three-dimensional ultrasound.[44] This is calculated using a manual or semiautomated planimetry and automated software called Virtual Organ Computer Aided Analysis (VOCAL).

By far the best correlation with implantation rates are being observed with power Doppler[43] and three-dimensional (3D) power Doppler studies (Fig. 29).[47-49] Ultrasound delineation and quantification of endometrial and subendometrial angiogenesis is emerging as a reliable and reproducible indicator of endometrial receptivity.[50,51] Basic static 3D and Virtual Organ Computer Aided Analysis (VOCAL) and 3D shell imaging have been used to assess and quantify endometrial and subendometrial vascularization.[47-49] The Vascularization Index (VI), Flow Index (FI) and Vascularization Flow Index of endometrial and subendometrial vessels increases during the proliferative phase, peaks 3 days prior to ovulation and decreases to a nadir 5 days postovulation.[49] VI is the ratio of color voxels to the total number of voxels inside the volume of interest and reflects the number of vessels in the volume being studied. FI is the flow index and is the ratio of the sum of color intensities to the number of color voxels inside the volume being interrogated. It reflects the amount of blood flow. VFI is the vascularization/flow index and is the ratio of the sum of color intensities to the total number of voxels inside the volume of interest. This reflects vessel presence and blood flow. Endometrial and subendometrial VI/FI/VFI is significantly, lower in stimulated cycles than in natural cycles.[48] Smoking is associated with significantly lower VI and VFI. Patients who become pregnant have a significantly lower Resistive Index (RI) of subendometrial vessels: 0.53

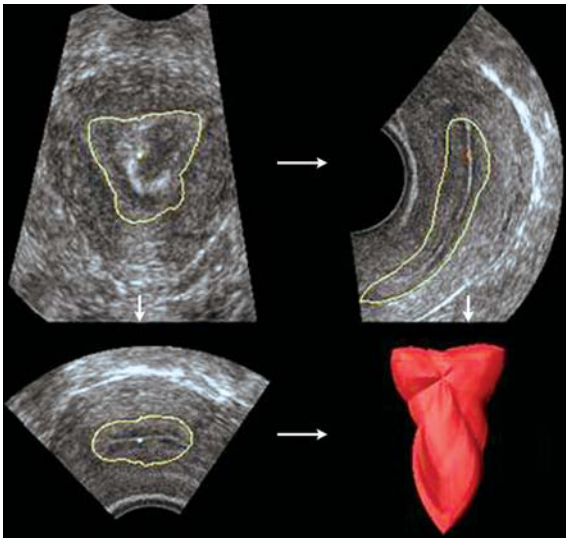

Fig. 28: Three-dimensional volume measurement of the endometrium. Using branded software called virtual organ computer aided analysis (VOCAL) the outline of the endometrium is traced through an acquired volume. The machine automatically calculates endometrial volume and displays it as shown in the bottom right hand picture. The other three frames show an orthogonal multiplanar display of the endometrium. The minimum volume associated with implantation is 1.59 ml

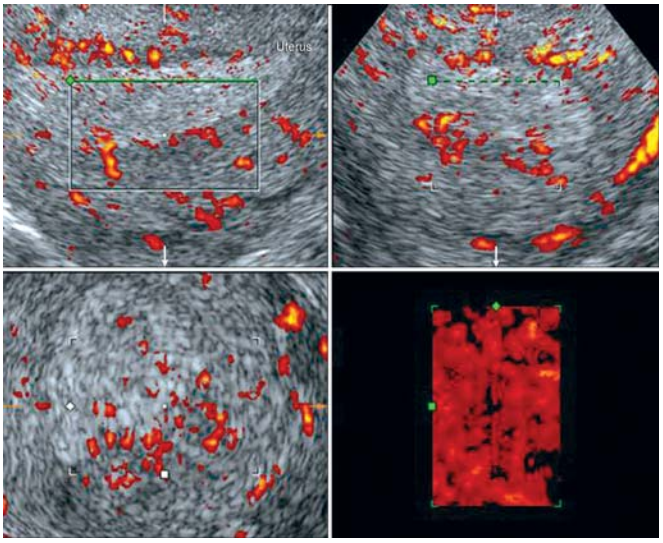

Fig. 29: Proliferation of spiral arteries and their subsequent growth into the endometrium is reflected as morphologic and quantitative increases in endometrial vascularity when imaged by power Doppler. This is seen in the late proliferative and periovulatory phases. The deeper the vascularization into the endometrium, the better the endometrial receptivity. 3D multiplanar studies with appropriate rendering afford an accurate delineation and quantification of angiogenesis in the endometrium. The illustration shows endometrial neovascularization in the longitudinal, axial and coronal planes alongwith the morphological rendering of endometrial vessels

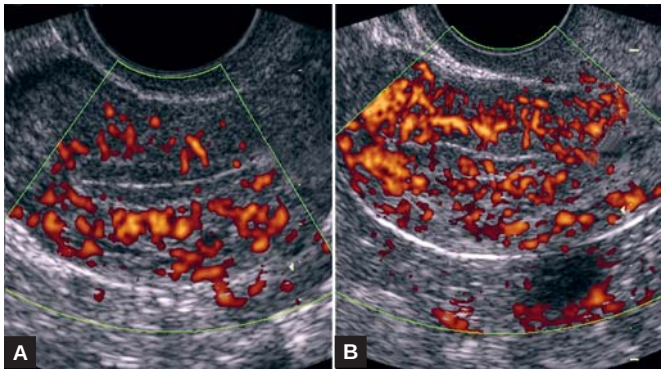

Figs 30A and B: Frame A shows vascularization into the midzone of the endometrium demonstrated by 2D power Doppler. Frame B shows extensive endometrial vascularization up to the cavity

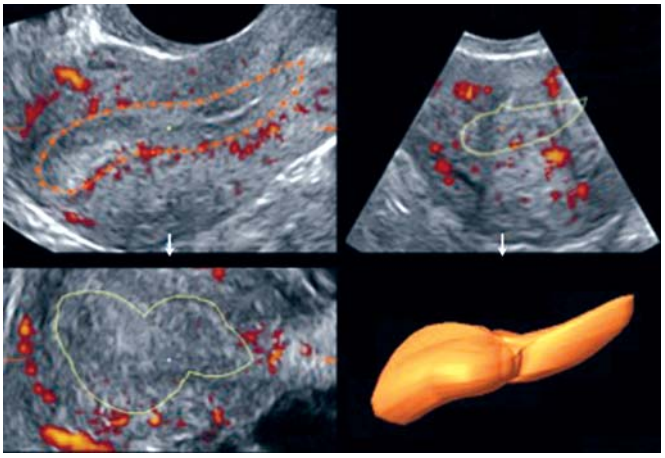

Fig. 31: 3D automated volume calculation (VOCAL) of the endometrium with calculation of 3D vascular indices

compared to 0.64 +/– 0.04 in pregnant and nonpregnant patients respectively.[47] Nondetectable subendometrial artery flo is not associated with a lower implantation rate.[44]

Inner zone vascularization (Figs 30A and B) of the endometrium observed on the day of hCG administration

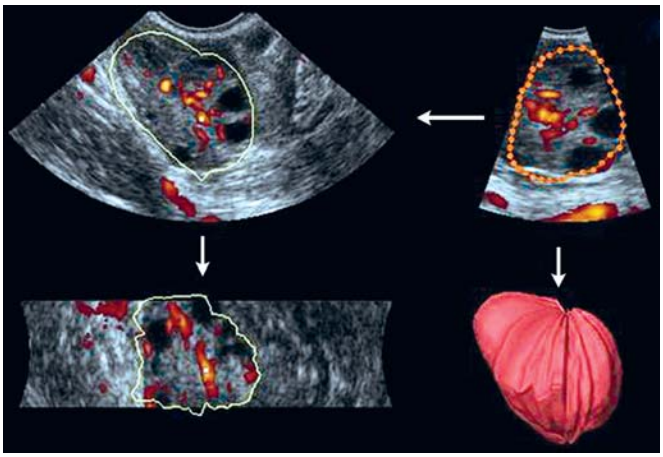

Fig. 32: Ovarian volume using three-dimensional acquisition techniques and three-dimensional quantification software is more accurate than 2D methods. However, volumes correlate well with embryo quality and fertilization rates but not with endometrial receptivity

Fig. 33: Grey scale and power Doppler acquisition of ovarian morphological data and stromal blood flow can be quantified using 3D software. Stromal blood flow correlates well with oocyte yield and embryo quality but not with implantation rates

or on the day of embryo transfer is associated with higher pregnancy rates. This can be assessed subjectively by direct observation but may be more objectively evaluated by quantification. Quantification can be done using the power Doppler area technique, which measures the vascularized area in any one endometrial plane or with VOCAL, which involves a 3D acquisition followed by semiautomated planimetry (Fig. 31). Preretrieval hCG does not enhance endometrial PI although more embryos are generated.[52] Interestingly, impedance in the uterine and spiral arteries does not show any significant difference between normal pregnancies, missed abortions and anembryonic pregnancies.[53]

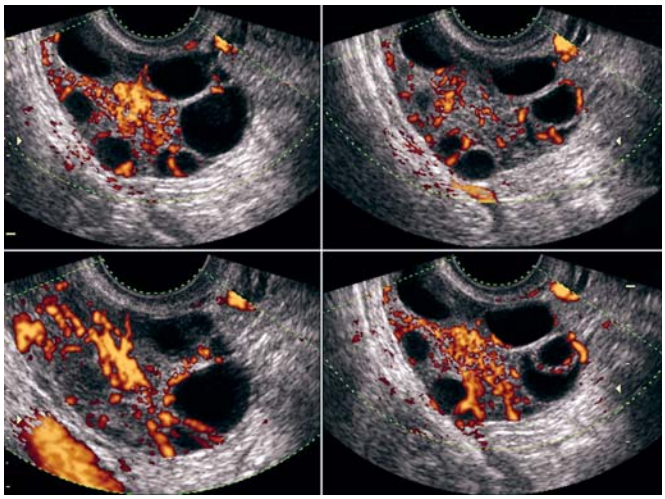

Fig. 34: Follicular maturation is accompanied by perifollicular neovascularization. This can be recognized by the appearance of occasional perifollicular vascular signals when the follicle reaches 12-14 mm in size, which then progress to 50-100% of perifollicular vascularization as the cycle progresses. This phenomenon correlates well with parameters of oocyte quality such as the levels of follicular fluid estradiol, pH, follicular fluid pO_2 and absence of oocyte aneuploidy. This neoangiogenesis, however, does not correlate well with endometrial receptivity

Ovarian antral follicle number, ovarian volume (Fig. 32), and ovarian stromal blood flow 3D quantification (Fig. 33) and 2D perifollicular vascularization(Fig. 34) correlate well with embryo quality and fertilization rates but do not have a direct correlation with endometrial receptivity.[48-50]

Fibroids

Fibroids are the most frequently encountered pathological finding on ultrasound. The number and location of fibroids is best assessed with 3D studies (Figs 35 to 37C). Fibroids are frequently multiple. Not infrequently, fibroids are large and a transabdominal and transvaginal approach may be necessary for adequate delineation. MRI may be useful in delineating very large fibroids from normal portions of the uterus and the ovaries.

Adenomyosis

Ectopic endometrial tissue in the myometrium is referred to as adenomyosis. The most frequent presenting symptom is heavy, painful periods with clots. Other manifestations include backache and infertility. Occasionally, the process may be clinically silent. The findings on 2D ultrasound are variable and numerous. These include focal or generalized myometrial thickening, diffuse or focal speckling, myometrial cysts and an obscured endometrial-myometrial

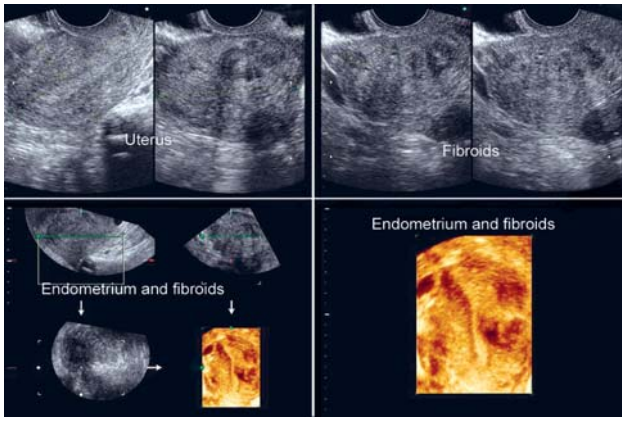

Fig. 35: Multiple fibroids are often difficult to localize on 2D transabdominal and transvaginal scans. 3D rendering demonstrates with great clarity the exact location of these fibroids and the extent of cavity components

Fig. 36A: Interstitial fibroids with a possible submucous component. 3D rendering clarifies the location as shown in figure 36B

Fig. 36B: Same patient as in figure 36A. 3D rendering shows a largely interstitial fibroid with a minimal submucous component. The other fibroid is not evident in this plane

Fig. 37A: Interstitial fibroid with a doubtful cavity component. 3D studies showed a better delineation and are shown in figures 37B and C

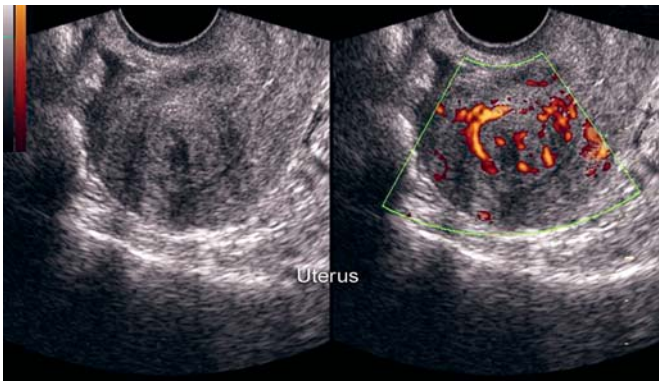

Fig. 38A: Focal subendometrial lesion. Differentiating this adenomyoma from a fibroid is possible with power Doppler studies. These reveal central vascularity with a spoke wheel radial pattern characteristic of an adenomyoma. Fibroids usually show only peripheral flow. Central flow in a fibroid is usually secondary to degeneration

Fig. 37B: 3D rendering shows the same fibroid as in figure 37A. The cavity is mildly displaced but the fibroid has no cavity component

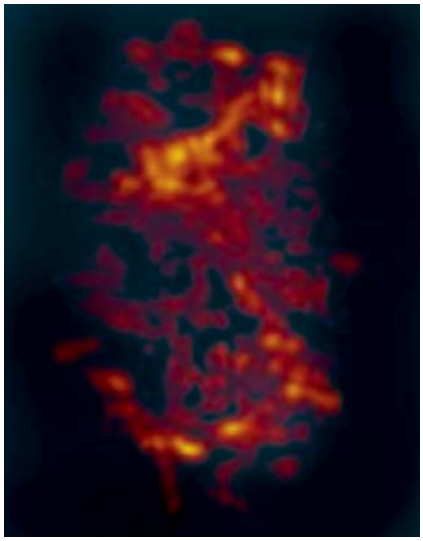

Fig. 38B: Power Doppler mapping reveals a spoke wheel pattern vascularity in the adenomyoma

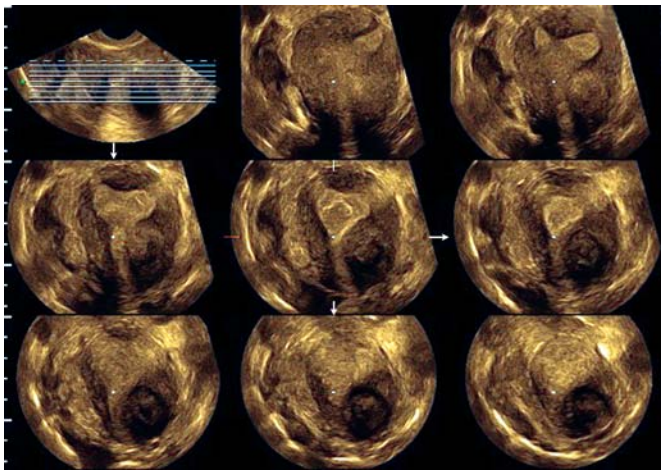

Fig. 37C: Tomographic ultrasound imaging demonstrates a lesion in multiple parallel planes. This makes it a useful modality for a more accurate delineation of the location of fibroids as shown in this entirely interstitial fibroid

junction. Myometrial thickening may be diffuse and present as an enlarged, globular uterus with a markedly increased transverse diameter or a differential thickening of the posterior wall and occasionally a differential thickening of the anterior wall. Sometimes, the process is focal and presents as a globular myometrial mass mimicking a fibroid. Differentiation is possible with the use of 3D Power Doppler which demonstrates the classical spoke wheel pattern of an adenomyoma (Figs 38A and B). This consists of a central vascular pool with radiating vessels and rim vascularization. Differentiation between fibroids and adenomyomas is important because management differs remarkably. Fibroids are handled with focal resection whereas adenomyomas do better with medical management or myolysis. Both lesions respond to GnRH analogues as a depot preparation.

The Fallopian Tubes

Healthy tubes are not visualized with 2D or 3D transvaginal scans. The interstitial part of the tubes is evident as an echogenic line extending towards the cornu from the cavity. Dilated tubes may be visualized depending on the extent, echogenecity and status of surrounding structures. Free fluid in the pelvis permits complete visualization of the tubes. These are seen as echogenic curvilinear structures engulfing the ovaries and are seen equally well on 2D and 3D scans. 3D scans are particularly useful for delineating adnexal organ relationships (Figs 39A to C) and for differentiating the tubal and ovarian components of the clinical tubo-ovarian mass (Figs 40A to E).

The Pelvic Peritoneum

The peritoneum serves as a useful window for systemic disease, for clues to pelvic pathology and for unusual diagnoses.

Hypoechoic fluid loculi of variable sizes are frequently seen in endometriosis. These may also be evident in non-specific pelvic inflammatory disease. Deep pelvic endometriosis is well visualized on 3D ultrasound but has to be specifically looked for.

Functional Ovarian Cysts

Cyclical changes in the ovary are prone to go into disarray and form cystic areas in the ovaries. Although referred to as functional cysts, these lesions are truly "dysfunctional" cysts. The clinical features are abnormal vaginal bleeding or pain, although some are entirely coincidental findings on an ultrasound examination. On ultrasound these are thin-walled and uniloculay. Internal echoes and peripheral vascularity may be evident. 3D images, although dramatic, rarely add diagnostic information to 2D observations. Care should be taken to differentiate between cysts of ovarian and paraovarian origin during transvaginal scanning and 3D is particularly useful for this.

Polycystic Ovaries

The Rotterdam ultrasound criteria for diagnosis include at least one of the following: an ovarian volume of greater than 10 cm^3 and the demonstration of 12 or more follicles 2 to 9 mm across (Figs 41A to D). If even one of the follicles exceeds 10 mm the study is to be repeated, when the ovaries are quiescent. The introduction of 3D "inversion mode" and "SonoAVC" software has revolutionized the objective evaluation of cystic spaces in the ovary. This finds widespread application in PCO assessment and in follicle monitoring. Data is acquired in the inversion mode, which

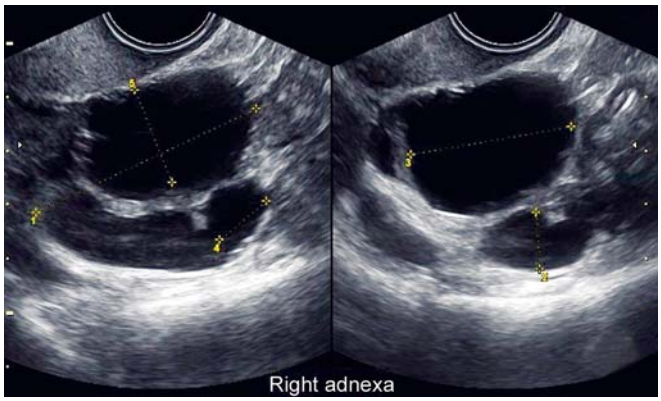

Fig. 39A: A classical tubo-ovarian mass consists of a fluid ovary surrounded by a fluid filled tube. Scan shows a lobulated fluid lesion in the ovary draped by a hydrosalpinx which is thin-walled and clear. See also figure 39B

Fig. 39B: Same patient as in Figure 39A. 3D rendering reveals a variably echogenic ovary surrounded by a multilocular hydrosalpinx. The texture of the walls of these lesions is best studied by 3D

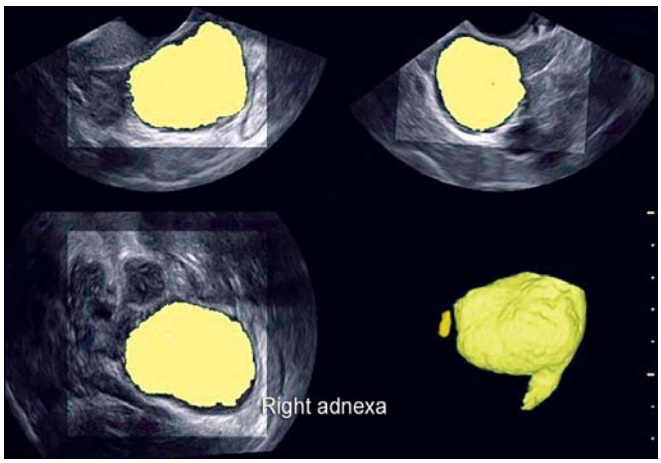

Fig. 39C: The SonoAVC software provided by one vendor automatically delineates fluid loculi with a color signal. This helps to highlight fluid collections anywhere in the body and can be used to delineate a hydrosalpinx as well

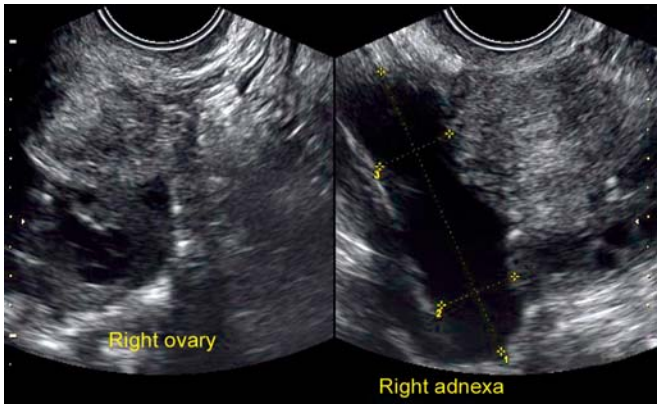

Fig. 40A: Transvaginal scan showing a hypoechoic right ovary and a tubular fluid loculus in the right adnexal. Further evaluation using 3D studies yielded information as shown in figures 40B and C

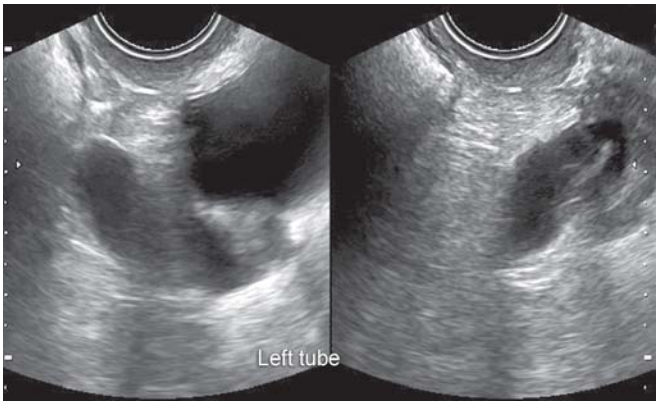

Fig. 40D: Transvaginal scan showing multiple hypoechoic and clear fluid loculation in the left adnexa. It is not possible to delineate the ovary from the tube

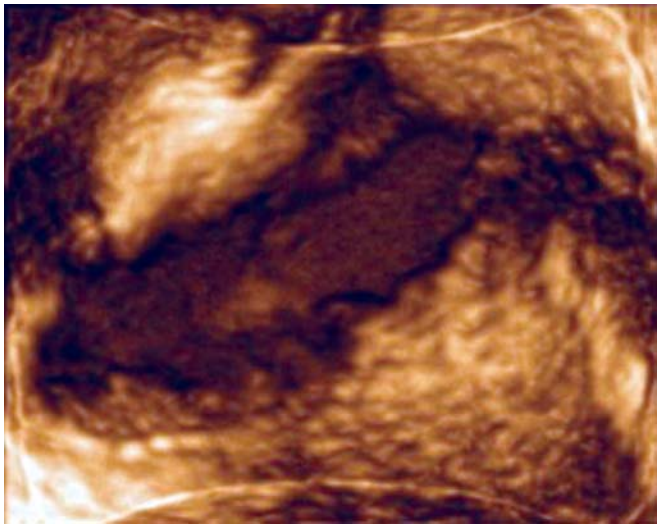

Fig. 40B: 3D reconstruction of the same patient as in figure 40A, the tubular structure is suggestive of a shaggy hydrosalpinx enveloping a corrugated ovarian surface

Fig. 40E: 3D reconstruction showing a distinct hydrosalpinx enveloping a globular ovary

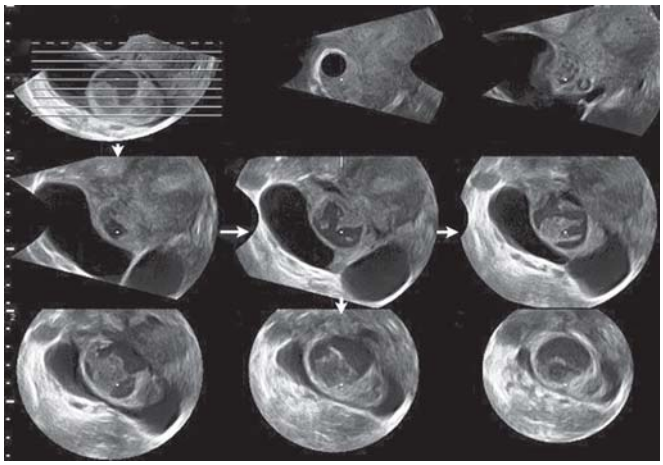

Fig. 40C: 3D tomographic ultrasound imaging of the same patient as in figures 40A and B. Sequential sections show a distinct hydrosalpinx enveloping an ovary, one edge of which shows echogenic debris, confirming acute salpingo-oophoritis

Fig. 41A: Polycystic ovaries are classically those which show a volume exceeding 10 cm^3 and 12 or more follicles 2-9 mm across. These strict criteria will exclude a large number of polycystic ovaries because the condition is influenced by associated endocrine disorders, treatment status and equipment resolution

Fig. 41B: Polycystic ovary showing a peripheral and central distribution of follicles. The older criterion for only peripheral distribution of follicles is no longer followed

Fig. 41C: Polycystic ovary showing the variant of largely central location of numerous follicles

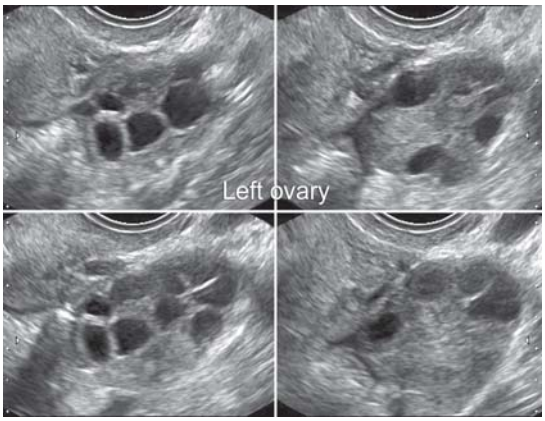

Fig. 41D: Scanning technique is important for delineating polycystic ovaries. 4 views of the same ovary are shown in this figure. Failure to scan the ovary from left to right and superior to inferior results in a suboptimal display of follicular number and distribution

reverses the gray scale and renders fluid as dark/colored and solid areas as voids. Activation of the SonoAVC function the tracks each cystic space and assesses diameters, volumes, location and total number of cysts/follicles (Figs 42A to E). Strict application of the Rotterdam criteria in day to day practice would miss a large number of polycystic ovaries. This is because the ultrasound morphology is influenced by several factors including transducer resolution, patient habitus, treatment status, associated hypothyroidism, hyperprolactinemia and incipient coexistent premature ovarian failure. The expanded ultrasound criteria in literature include stromal hyperplasia assessed subjectively and by 3D, increased stromal echogenecity assessed subjectively, stromal hyperemia assessed with 3D power Doppler studies and peripheral, central or random distribution of excessive number of follicles. 2D and 3D power Doppler indices correlate well with fertility outcomes but are not consistent diagnostic criteria.[50]

Ovarian Hyperstimulation

Ovulation induction with gonadotrophins and occasionally even with clomiphene citrate can result in enlarged ovaries with multiple follicles, multiple corpora lutea and varying severity of increased capillary permeability manifesting as ascites and pleural effusion. The SonoAVC function is very useful to quantify the size and number of cysts.

Premature Ovarian Failure

Although premature ovarian failure is essentially a diagnosis made by serum follicle stimulating hormone (FSH) estimations, ultrasound is useful for guiding the diagnosis and assessing ovarian reserve inpatients desirous of beating the body clock. The ovaries shrink in volume to less than 3.0 ml and there is a paucity of antral follicles. The antral follicle count which is a good predictor of *in vitro* fertilisation (IVF) treatment cycles can be extrapolated for the diagnosis of ovarian failure. Transvaginal scans done on day 3,4 or 5 of the cycle reveal less than 4 antral follicles in the ovaries. 3D evaluation with inversion mode and the SonoAVC function is superior to a subjective 2D sweep.

Neoplastic Ovarian Masses

One of the main aims of gynecological ultrasound is early identification of malignant ovarian masses in order to improve outcomes. Early detection improves 5 year survival rates from 30 to 35% in stage III and stage IV disease to 80 to 85% in stage I disease. Neoplastic ovarian masses have a wide pathological spectrum and vary in appearance from

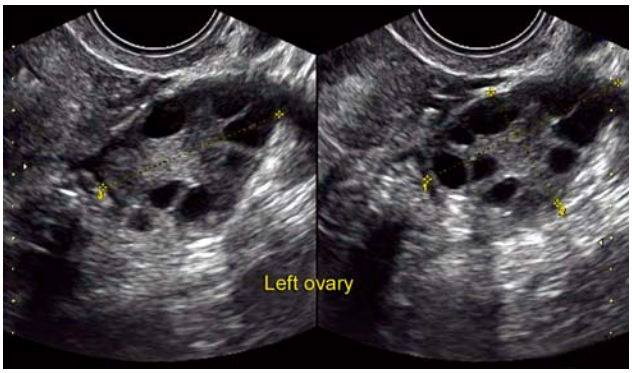

Fig. 42A: Polycystic ovary showing multiple peripherally located abundant follicles and excessive stroma. Figures 42B to E show further evaluation of this ovary

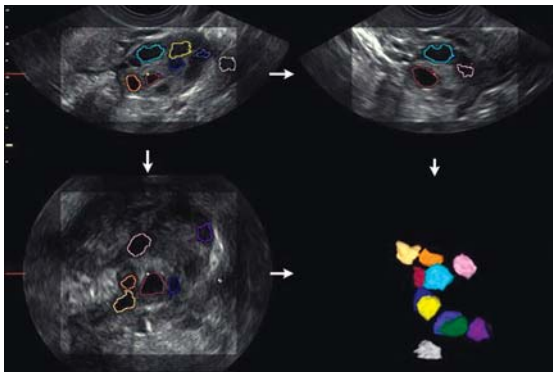

Fig. 42D: Same patient as in figure 42A showing a 3D graphic display of the contralateral ovary

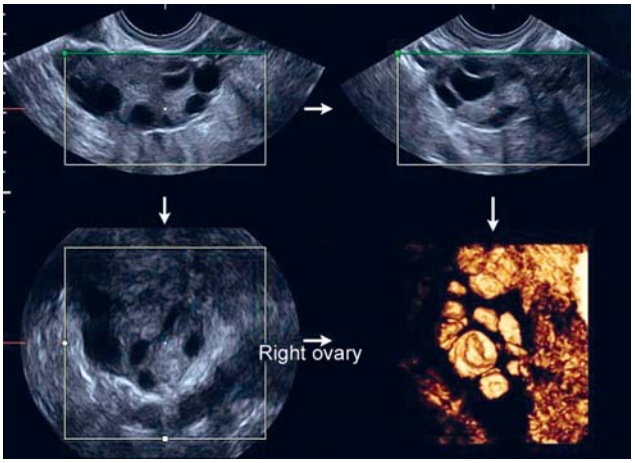

Fig. 42B: Same case as in figure 42A. A 3D acquisition has been made of the entire ovary and displayed in three orthogonal planes. Frame D shows a 3D inversion mode rendering. Using this method, follicles are highlighted and the stroma blacked out. This improves the appreciation of the number and distribution of follicles

Name								Perf. Phys.						
Pat. ID				DOB				Ref. Phys.						
Indication				Sex				Sonogr.						
LMP				Day of Cycle				Gravida				AB		
Day of stim.				Expected Ovul.				Para				Ectopic		
Ovary:	Left							Ovary:	Right					
Total#:	11							Total#:	14					
Nr.	d(V) mm	dx mm	dy mm	dz mm	mn. d mm	V cm³		Nr.	d(V) mm	dx mm	dy mm	dz mm	mn. d mm	V cm³
1	7.3	8.7	7.3	6.4	7.5	0.20		1	9.9	14.0	12.4	7.3	11.2	0.51
2	7.1	9.0	8.4	5.2	7.5	0.19		2	8.3	11.5	9.7	5.5	8.9	0.30
3	6.7	8.1	7.4	6.3	7.3	0.16		3	7.3	8.1	7.7	6.3	7.4	0.20
4	6.6	9.9	6.9	5.5	7.4	0.15		4	6.6	8.9	6.1	5.5	6.8	0.15
5	6.5	8.7	6.8	5.1	6.9	0.14		5	6.4	8.8	7.3	4.9	7.0	0.14
6	6.4	10.8	7.7	3.8	7.4	0.13		6	6.3	8.0	7.3	6.0	7.1	0.13
7	6.2	8.5	6.6	5.1	6.8	0.12		7	6.3	8.8	6.6	4.7	6.7	0.13
8	6.2	8.6	6.6	4.8	6.7	0.12		8	5.6	7.8	6.9	4.2	6.3	0.09
9	6.2	8.3	7.2	4.3	6.6	0.12		9	5.6	7.7	6.2	4.6	6.2	0.09
10	5.7	8.7	5.8	4.0	6.1	0.10		10	5.6	9.1	5.6	3.9	6.2	0.09
11	5.7	8.9	5.7	4.1	6.2	0.10		11	5.5	9.4	6.3	3.1	6.3	0.09
								12	4.9	6.4	5.7	3.3	5.1	0.06
								13	4.8	7.2	5.1	3.4	5.3	0.06

Fig. 42E: Automated report of follicular size and number of the same patient as in figure 42A. The report shows color coding of each follicle, the three dimensions of each follicle and the mean diameter of each follicle

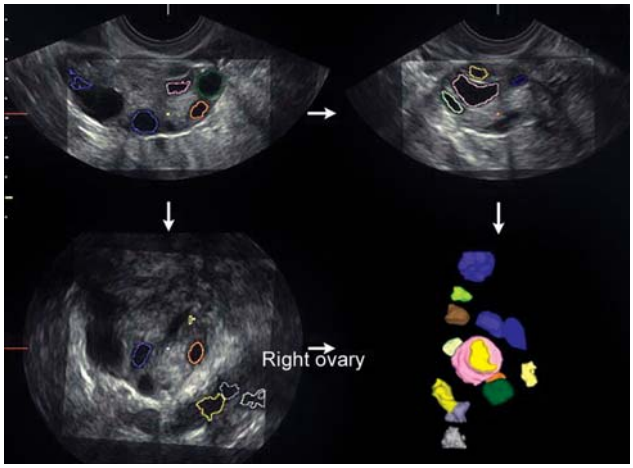

Fig. 42C: The calculation of follicle number can be automated using proprietary 3D software. In this technique, the ovary is chosen as the region of interest and the appropriate software choice key is activated on the equipment console. The software automatically assesses the size and number of follicles and allots a different color to each follicle. Frame D shows a color coded display of the polycystic ovary shown in section planes A, B and C

simple, thin walled, unilocular, avascular cysts to completely solid masses. Advances in transducer technology, color Doppler, power Doppler and 3D studies have greatly enhanced the accuracy of histological prediction of benign and malignant adnexal lesions.[54,55] The criteria for a diagnosis of a malignant mass include grey scale observations of a solid mass, a cystic mass with solid areas, focal or diffusely thick walls or septations, mural nodules and heterogeneous internal echoes. Pelvic and paraaortic lymph nodes enlargement, ascites, suprarenal and liver metastases and pleural effusions can be elucidated by transabdominal ultrasound. Color flow and 3D vascular reconstruction criteria include abnormal calibration of vessels, dichotomous branches, elongation, coiling, aneurysms, vascular lakes, arteriovenous anastamoses and veno-venous anastomoses (Figs 43 to 50). Low resistive and pulsatility indices are inadequately wide-range to be reliable. Serial evaluation using 3D power Doppler quantification are also proving useful for following up patients on treatment, particularly those on antineoangiogenesis agents.

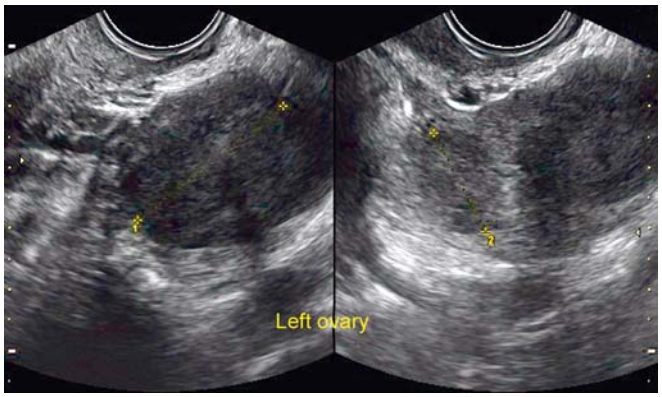

Fig. 43: Solid ovarian lesions as seen in this ovary are not necessarily malignant and the 2D morphology needs to be supplemented with color and 3D color criteria for histologic characterization as shown in figures 49 and 50

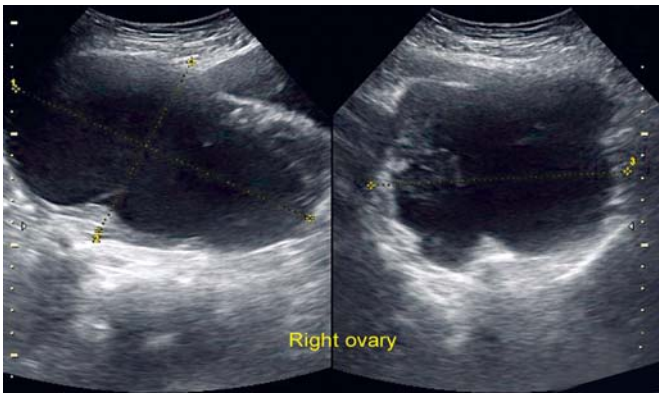

Fig. 46: Shaggy lesions with echogenic fluid contents usually indicate old benign hemorrhagic lesions or mucinous neoplasm. The latter are often avascular and difficult to characterize. Magnetic resonance imaging is sensitive to iron content of lesions and helps to differentiate hemorrhagic lesions from those that do not contain blood

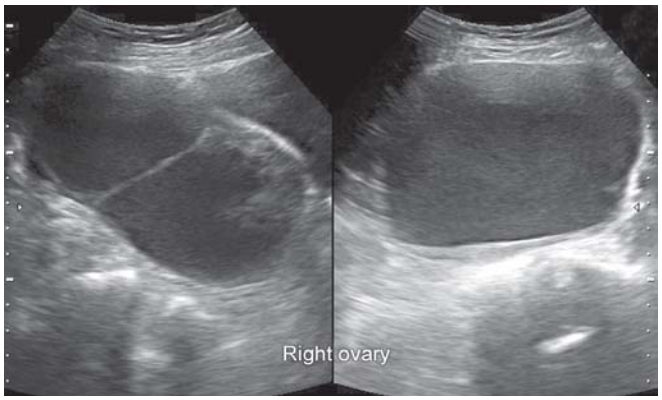

Fig. 44: Echogenic cystic lesions with thin septations are usually benign hemorrhagic lesions. Occasionally, however, these may be pathologic surprises and should be assessed with power and color Doppler to confirm a benign pattern as shown in figure 50

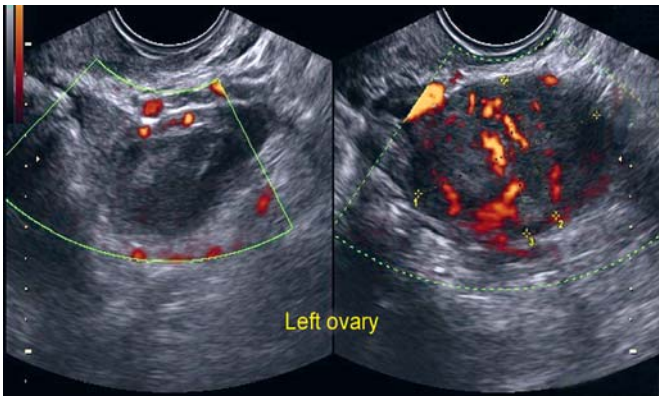

Fig. 47: All solid lesions should be assessed with power Doppler. The presence of vascularity within a solid lesion confirms the presence of tissue and excludes fluid. This is a useful criterion for a neoplastic lesion. Occasionally, benign granulation tissue such as within an abscess may mimic this finding. A clinical perspective is therefore useful in the interpretation of these findings

Fig. 45: Cystic lesions with thick septations and mural nodules are highly suspicious for malignancy on 2D criteria alone

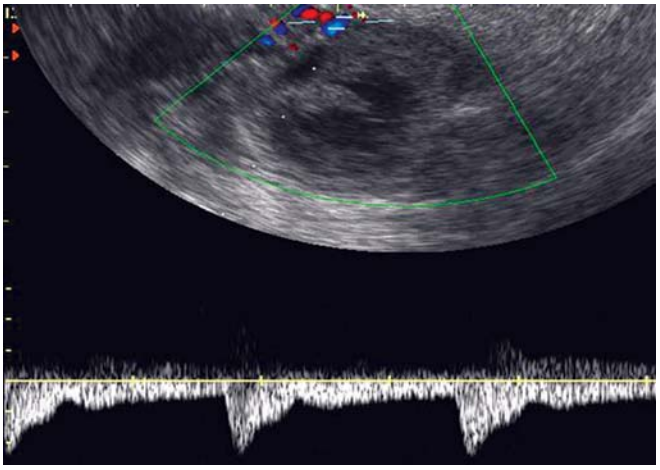

Fig. 48A: Spectral Doppler is often misleading in characterizing adnexal lesions. This is so because vessels in the periphery of the lesion are usually host vessels and may not show low impedance characteristics. Intratumoral vessels are low impedance circuits because tumor neoangiogenesis usually gives rise to vessels that lack muscle in their walls

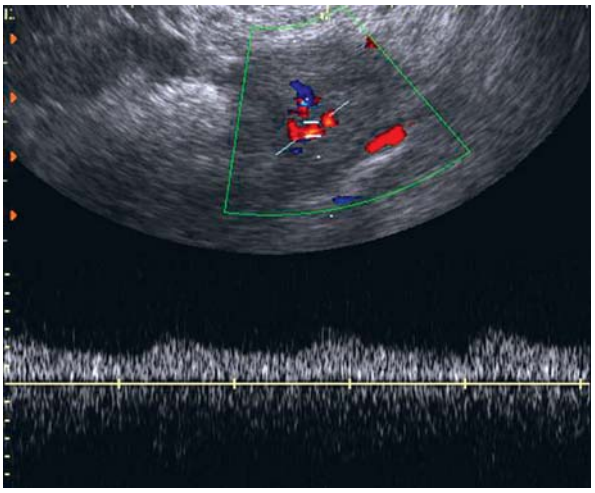

Fig. 48B: Classical low impedance flow in the center of a malignant mass. Some workers quantify cut-offs at a resistive index of 0.40 and others at 0.33. Specific figures should be disregarded and emphasis laid on morphology as detailed in the text

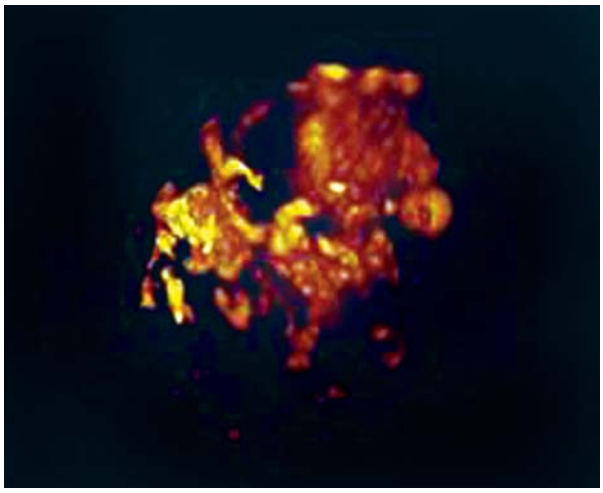

Fig. 49C: Same lesion as in figure 48B. Note the aneurysmal dilatation of vessels and the vascular lakes characteristic of malignant lesions

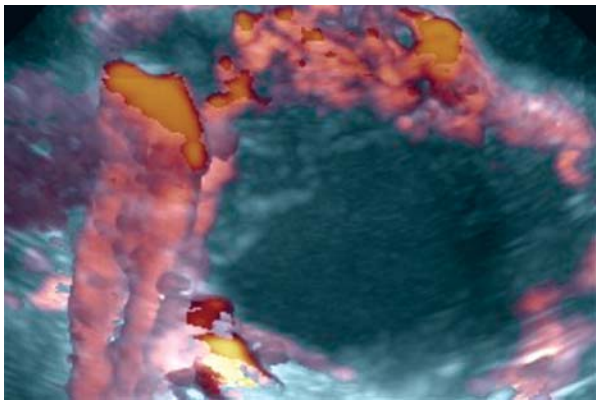

Fig. 49A: Markedly tortuous vessels with extensive coiling in a mucinous cystadenocarcinoma

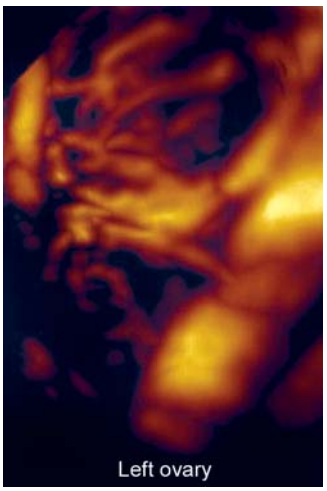

Fig. 49D: Cluster of abnormal vessels showing bizarre sizes. These features indicate a malignant lesion

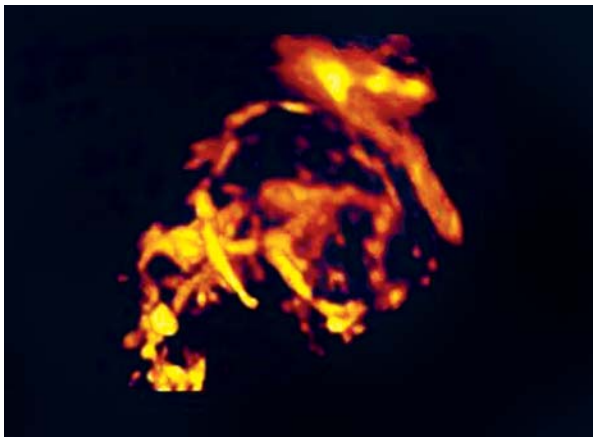

Fig. 49B: Tortuous vessels with abnormal caliber in a malignant mass. In a benign lesion, larger vessels give rise to narrower vessels. In malignant lesions, second, third and higher-order branches are often wider than the parent vessels. Note also that several also larger vessels are giving rise to multiple branches at a single point. This type of branching is a characteristic of malignant lesion. Benign lesions show a single branch at a time

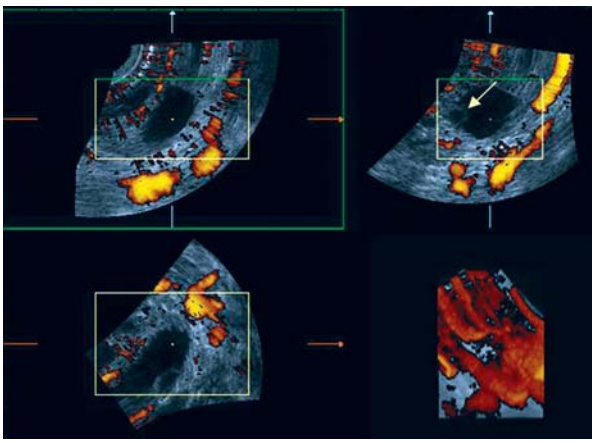

Fig. 49E: Small cystic lesions throwing up a surprise on 3D power Doppler. The 3D rendering shows a bizarre branching pattern suggesting malignancy which was confirmed after surgery

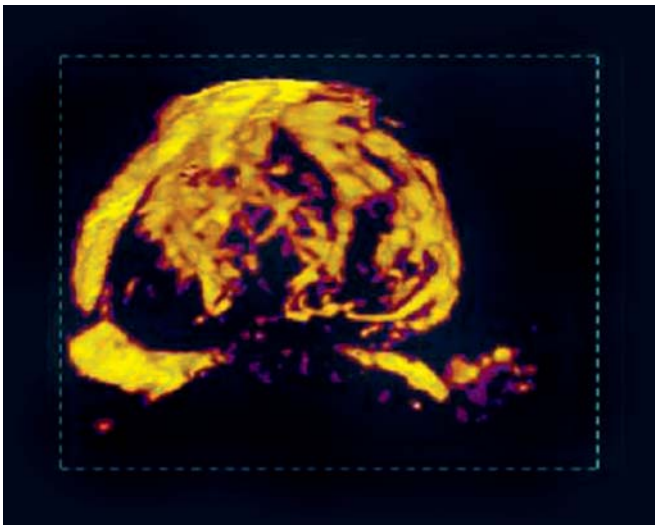

Fig. 49F: Central spoke-wheel pattern in a solid adnexal mass seen on 3D rendered studies. Surgical pathology confirmed a malignant fibroma

Miscellaneous Adnexal Lesions

Several extraovarian adnexal lesions are found on transvaginal scans and many of these are of no clinical consequence. Paraovarian cysts are thin-walled, clear, avascular cystic lesions. These may be unilocular or multilocular (Figs 51A and B). 3D enhances the detection of para-ovarian and extraovarian location of adnexal cysts. Other thin-walled cystic lesions include paratubal cysts, fimbrial cysts and cysts of Morgagni. Pelvic kidneys may masquerade as solid pelvic lesions. Subserous fibroids may be indistinguishable from solid adnexal lesions. Inflammatory bowel lesions such as diverticulitis, appendicitis and focal enteritis may masquerade as gynecological lesions.

Ultrasound in Urogynecology

Recent years have seen ultrasound images replace conventional radiology as the modality of choice for imaging

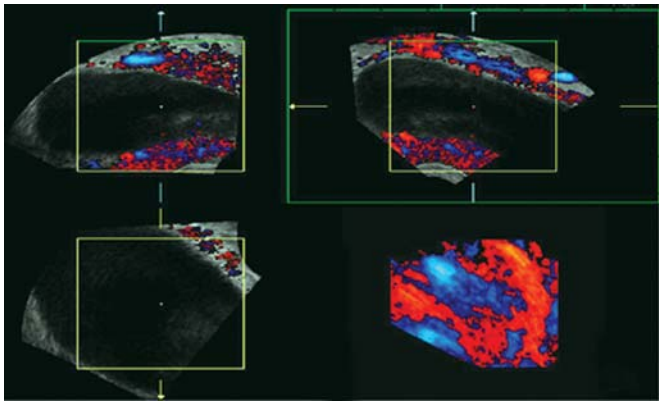

Fig. 49G: Unilocular cystic lesions showing a thick vascular wall on 3D studies. The 3D rendering shows arteriovenous anastamoses. Surgery confirmed a serous cystadenocarcinoma

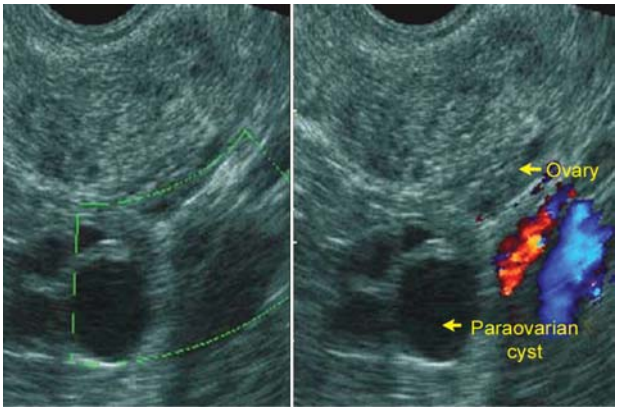

Fig. 51A: Paraovarian cysts are best characterized by demonstrating the ovary separate from them

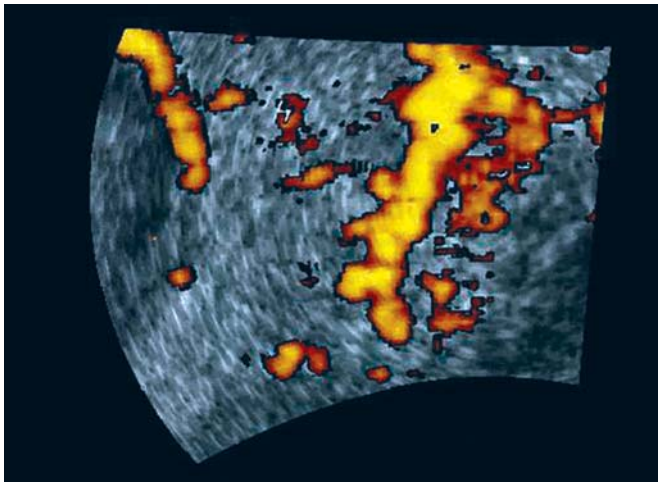

Fig. 50: Benign vessel showing one branch at a time. Note the regular decrease in the size of this feeder vessel as it goes towards the center of the solid lesion. Surgery confirmed a benign fibroma

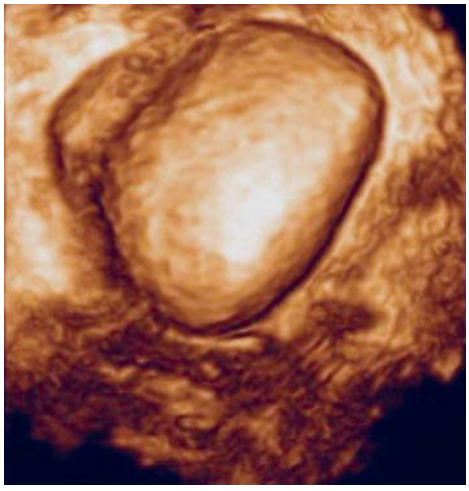

Fig. 51B: 3D reconstructions are particularly useful for demonstrating the spatial relationships of adnexal structures. Figure shows a normal ovary with an adjacent large paraovarian cyst

the female patient with a voiding dysfunction. This is consequent to remarkable technological advances combined with innovative techniques of obtaining relevant morphological and dynamic information. Transabdominal ultrasound has now been complemented by a wide variety of ultrasound techniques, which include transurethral ultrasound, introital ultrasound, perineal ultrasound, endoanal and transectal scanning, power Doppler information and 3D and 4D technology.

Transvaginal, introital and perineal ultrasound can all be performed with the same transducer. This should be an end-firing intracavitary transducer with an emission angle of at least 90°. The availability of higher frequencies up to 12 MHz will permit better resolution of superficial structures and the use of lower frequencies such as 5 MHz will allow a better assessment of large pelvic masses and a very large uterus.

Whereas, magnetic resonance imaging (MRI) has been the modality for visualizing the endopelvic fascia, in recent years 3D ultrasound sectional images are replacing MRI (Fig. 52) because of an equivalent resolution (Figs 53 and 54) and the added advantage of ease of utility and the ability for vascular display. Anatomical atrophy of the endopelvic fascia, change in the configuration of the vagina (Fig. 55)

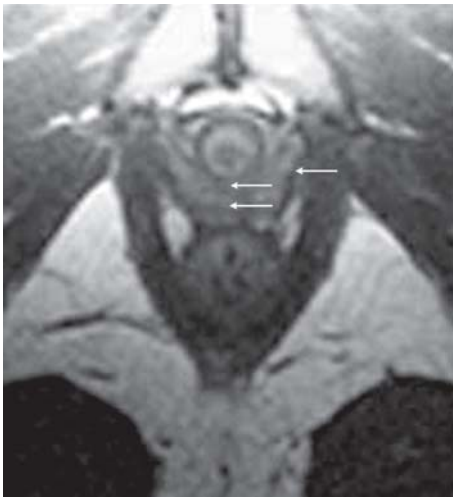

Fig. 52: Magnetic resonance image (MRI) of the pelvis showing in the midline, the urethra anteriorly, the pubocervical ligament (two arrows), the levator ani (single arrow), the vagina and rectum

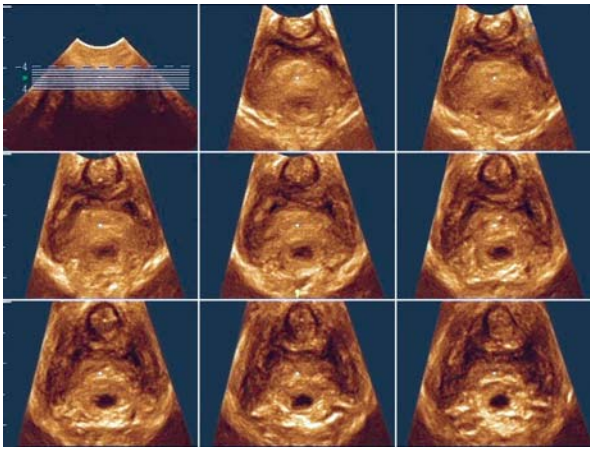

Fig. 54: 3D Tomographic ultrasound imaging (TUI). Currently available 3D transducers acquire information in sweeps across the region of interest. Each signal thus acquired can be rendered in an infinite number of planes. TUI allows a choice of plane direction and thickness in much the same format as CT or MRI. Note the exquisite soft tissue detail of the urethra, vagina, rectum and endopelvic fascia. The vagina has an H-shaped configuration as evident in sections 1-4

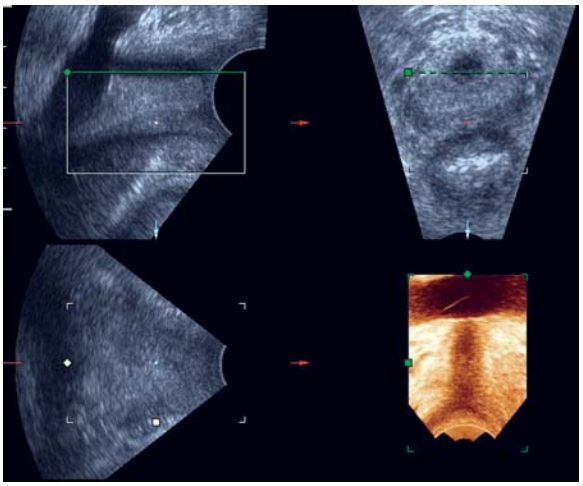

Fig. 53: Three-dimensional (3D) images of the endopelvic fascia showing the region in three orthogonal planes and one rendered plane. The top left image shows (from top to bottom) the urethra, vagina and rectum in the midline and the fibromuscular tissue laterally. The rendered image (bottom right) shows the urethra flanked by the endopelvic fascia

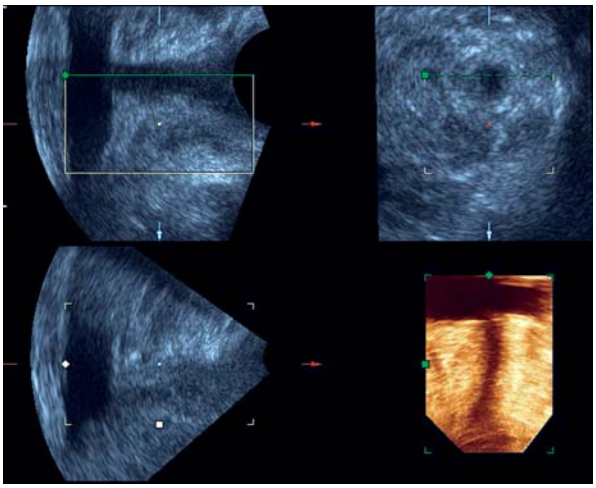

Fig. 55: Complete loss of anatomical delineation of the vagina, rectum and endopelvic fascia in postmenopausal atrophy in a patient with incontinence. The difference is striking when the plane displayed in the top right area is compared with its counterpart in figure 53

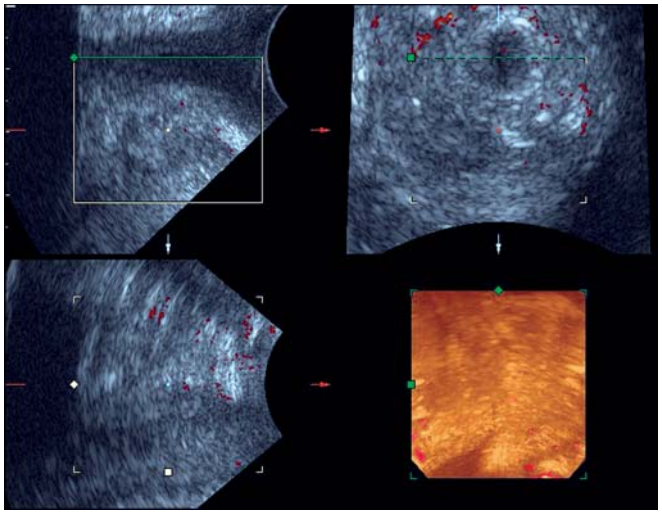

Fig. 56: 3D tomographic ultrasound imaging with grey scale and power Doppler information. Note the scanty vascular signals seen in the top right image and the complete absence of vascular signals in the other orthogonal planes

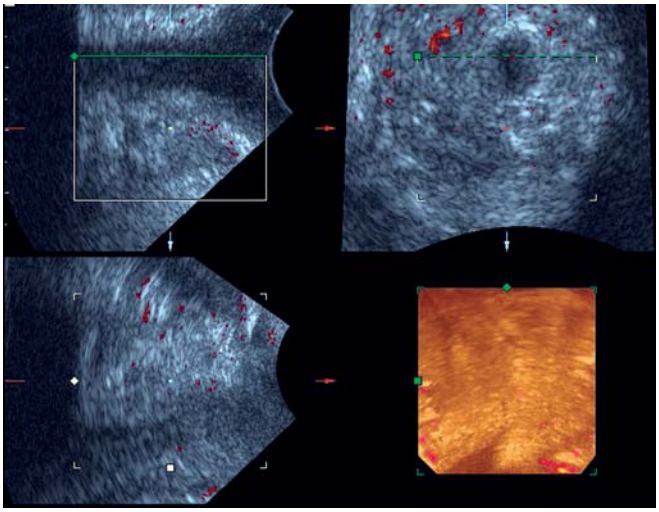

Fig. 57: 3D tomographic ultrasound imaging with 2D and power Doppler information in a patient on perineal exercises and local estrogen cream application. Note the increased vascular signals in the top right frame when compared with figure 55

and paucity of vasculature (Fig. 56) can be documented with amazing clarity and reproducibility. Vascular response to perineal exercises and local estrogen application (Fig. 57) can be demonstrated by serial scans done 6 to 12 weeks apart. Transanal and transrectal side-firing linear transducers now offer detailed delineation of the anal and urethral sphincters and sphincter mechanisms and in the future are likely to find increased application. 3D provides objective evaluation of outcomes from urethral bulking agent therapy using collagen injections[56] and helps in assessing failure and the need for reinjection. Tension free vaginal tape slings are highly echogenic and can be assessed by 3D ultrasound.[57] Tape movement occurs in an arc around the posterior aspect of the posterior symphysis which serves as the fulcrum. Mechanical compression of the urethra by the tape is evident as a reduction in the gap between the tape and the symphysis pubis.

CONCLUSION

Until less than a decade ago, reports of three-dimensional ultrasound (3D) and real-time three-dimensional ultrasound (4D) were fraught with inconsistencies of outcomes, inconsistencies of method, personal bias, skeptical overtones, and had a dramatic but often unrecognizable lack of declaration of the degree of technical sophistication of the equipment used. As a consequence, the utility of the technique as a component of good clinical practice remained unacknowledged. The scenario today has changed completely. The techniques are established as a yardstick of morbid anatomy and pathophysiology.

REFERENCES

1. Kupesic S, Kurjak A, Bjelos D. Sonographic imaging in infertility. In Kurjak A, Chervenak FA (Eds). Donald school textbook of ultrasound in Obstetrics and Gynecology (1st ed). New Delhi: Jaypee Brothers Medical Publishers, 2003;658-90.
2. Ashton D, Amin HK, Richart RM, Neuwirth RS. The incidence of asymptomatic uterine anomalies in women undergoing transcervical tubal sterilization. Obstet Gynecol 1988;72:28-30.
3. Sorenson S. Estimated prevalence of mulerian anomalies. Acta Obstet Gynecol Scand 1988;67:441-45.
4. Heinonen PK, Saarikoski S, Pystynen P. Reproductive performance of women with uterine anomalies. An evaluation of 182 cases. Acta Obstet Gynecol Scand 1982;61:157-62.
5. Fedele L, Bianchi S, Marchini M, Franchi D, Tozzi L, Dorta M. Ultrastructural aspects of endometrium in infertile women with septate uterus. Fertil Steril 1996;65:750-52.
6. Fedele L, Arcaini L, Parazzini F, Vercellini P, Nola GD. Metroplastic hysteroscopy and fertility. Fertil Steril 1993; 59:768-70.
7. Valdes C, Malini S, Malinak LR. Ultrasound evaluation of female genital tract anomalies: A review of 64 cases. Am J Obstet Gynecol 1984;149:285-90.
8. Cararach M, Penella J, Ubeda J, Iabastida R. Hysteroscopic incision of the septate uterus: Scissors versus resectoscope. Hum Reprod 1994;9:87-89.
9. Goldenberg M, Sivan E, Sharabi Z. Reproductive outcome following hysteroscopic management of intrauterine septum and adhesions. Hum Reprod 1995;10:2663-65.
10. The American Fertility Society. The American Fertility Society classifications of adnexal adhesions, distal tubal occlusion, tubal occlusion secondary to tubal ligation, tubal pregnancies, mullerian anomalies and intrauterine adhesions. Fertil Steril 1988;49(6):944-55.
11. Homer HA, Li TC, Cooke ID. The septate uterus: A review of management and reproductive outcome. Fertil Steril 2000;73: 1-4.

12. La Torre R, Prosperi Porta R, Franco C, Sansone M, Mazzocco M, Pergolini I, De Felice C, Cosmi EV. Three-dimensional sonography and hysterosalpingosonography in the diagnosis of uterine anomalies. Clin Exp Obstet Gynecol 2003;30(4):190-92.
13. Nicolini U, Belloti M, Bonazzi B, Zamberletti D, Candiani GB. Can ultrasound be used screen uterine malformations? Fertil Steril 1987;47:89-93.
14. Reuter KL, Daly DC, Cohen SM. Septate versus bicornuate uteri: Errors in imaging diagnosis. Radiology 1989;172:749-52.
15. Randolph J, Ying Y, Maier D, Schmidt C, Riddick D. Comparison of real time ultrasonography, and laparoscopy/hysteroscopy in the evaluation of uterine abnormalities and tubal patency. Fertil Steril 1986;5:828-32.
16. Bega G, Lev-Toaff AS, O'Kane P, Becker E Jr, Kurtz AB. Three-dimensional ultrasonography in Gynecology: Technical aspects and clinical applications. J Ultrasound Med 2003;22(11): 1249-69.
17. Salle B, Sergeant P, Galcherand P, Guimont I, De Saint Hilaire P, Rudigoz RC. Transvaginal hysterosonographic evaluation of septate uteri: A preliminary report. Hum Reprod 1996;11: 1004-07.
18. Kupesic S, Kurjak A. Septate uterus: Detection and prediction of obstetrical complications by different forms of ultrasonography. J Ultrasound Med 1998;17:631-36.
19. Richman TS, Viscomi GN, Cherney AD, Polan A. Fallopian tubal patency assessment by ultrasound following fluid injection. Radiology 1984;152:507-10.
20. Marshall C, Mintz DI, Thickman D, Gussman H, Kressel Y. MR evaluation of uterine anomalies. Radiology 1987;148: 287-89.
21. Carrington BM, Hricak M, Naruddin RN. Mullerian duct anomalies: MR evaluation. Radiology 1990;170:715-20.
22. Raga F, Bonilla-Musoles F, Blanes J, Osborne NG. Congenital Mullerian anomalies: Diagnostic accuracy of three-dimensional ultrasound. Fertil Steril 1996;65(3):523-28.
23. Wu MH, Hsu CC, Huang KE. Detection of congenital mullerian duct anomalies using three-dimensional ultrasound. J Clin Ultrasound 1997;25:487-92.
24. Jurkovic D, Giepel A, Gurboeck K, Jauniaux E, Natucci M, Campbell S. Three-dimensional ultrasound for the assessment of uterine anatomy and detection of congenital anomalies: A comparison with hysterosalpingography and two-dimensional sonography. Ultrasound Obstet Gynecol 1995;5:233-37.
25. Dabrashrafi H, Bahadori M, Mohammad K, Alavi M, Moghadami-Tabrizi N, Zandinejad R. Septate uterus: New idea on the histologic features of the septum in this abnormal uterus. Am J Obstet Gynecol 1995;172:105-07.
26. Kupesic S, Kurjak A, Skenderovic S, Bjelos D. Screening for uterine abnormalities by three-dimensional ultrasound improves perinatal outcome. J Perinat Med 2002;30:9-17.
27. Weinraub Z, Maymon R, Shulman A, Bukovsky J, Kratochwil A, Lee A, Herman A. Three-dimensional saline contrast rendering of uterine cavity pathology. Ultrasound Obstet Gynecol 1996;8(4):277-82.
28. Balen FG, Allen CM, Gardener JE, Siddle NC, Lees WR. 3-dimensional reconstruction of ultrasound images of the uterine cavity. The British Journal of Radiology 1993;66(787):588-91.
29. Salim R, Regan L, Woelfer B, Backos M, Jurkovic D. A comparative study of the morphology of congenital uterine anomalies in women with and without a history of recurrent first trimester miscarriage. Human Reproduction 2003; 18(1):162-66.
30. Salim R, Woelfer B, Backos M, Regan L, Jurkovic D. Reproducibility of three-dimensional ultrasound diagnosis of congenital uterine anomalies. Ultrasound Obstet Gynecol 2003;21(6):578-82.
31. Kupesic S, Kurjak A. Three-dimensional ultrasound and power Doppler assessment of the septate uterus. In Kurjak A (Eds). Three dimensional power Doppler in Obstetrics and Gynecology (1st ed). New York: Parthenon Publishing, 2000;85-91.
32. Khurana A. The endometrium. In Khurana A, Dahiya N (Eds). 3D and 4D Ultrasound: A text and Atlas (1st ed). New Delhi: Jypee Brothers Medical Publishers, 2004;166-98.
33. Delisle MF, Villeneuve M, Boulvain M. Measurement of endometrial thickness with transvaginal ultrasonography: Is it reproducible? J Ultrasound Med 1998;17:481-84.
34. Buyuk E, Durmusoglu F, Erenus M, Karakoc B. Endometrial disease diagnosed by transvaginal ultrasound and dilatation and curettage. Acta Obstet Gynecol 1999;79:419-22.
35. Jorizzo JR, Riccio GJ, Chen MYM, Carr JJ. Sonohysterography: the next step in the evaluation of the abnormal endometrium. Radiographics 1999;119:S117-S30.
36. Weigel M, Friese K, Strittmatter HJ, Melchert F. Measuring the thickness: Is that all we have to do for sonographic assessment of endometrium in postmenopausal women. Ultrasound Obstet Gynecol 1995;6(2):97-102.
37. Sousa R, Silvestre M, Almeida e Sousa L, Falcao F, Dias I, Silva T, De Oliveira C, Oliveira HM. Transvaginal ultrasonography and hysteroscopy in postmenopausal bleeding: A prospective study. Acta Obstet Gynecol Scan Sep 2001;80(9): 856-62.
38. Goldstein RB, Bree RL, Benson CB, Benacerraf BR, Bloss JD, Carlos R, Fleischer AC, Goldstein SR, Hunt RB, Kurman RJ, Kurtz AB, Laing FC, Parsons AK, Smith-Bindman R, Walker J. Evaluation of the woman with postmenopausal bleeding: Society of Radiologists in Ultrasound-Sponsored Consensus Conference statement. J Ultrasound Med Oct 2001;20(10): 1025-36.
39. Epstein E, Valentin L. Rebleeding and endometrial growth in women with postmenopausal bleeding and endometrial thickness <5 mm managed by dilatation and curettage or ultrasound follow-up: A randomized controlled study. Ultrasound Obstet Gynecol Nov 2001;18(5):499-504.
40. Randelzhofer B, Prompeler HJ, Sauerbrei W, Madjar H, Emons G. Value of sonomorphological criteria of the endometrium in women with postmenopausal bleeding: A multivariate analysis. Ultrasound Obstet Gynecol Jan 2002;19(1):62-68.
41. Sheikh M, Sawhney S, Khurana A, Al-Yatama M. Alteration of sonographic texture of the endometrium in postmenopausal bleeding: A guide to further management. Acta Obstet Gynecol Scand 2000;79:1006-10.
42. Pierson RA. Imaging the endometrium: Are there predictors of uterine receptivity? J Obstet Gynaecol Can 2003;25(5):360-68.
43. Baruffi RL, Contart P, Mauri AL, Peterson C, Felipe V, Garbellini E, Franco JG. A uterine ultrasonographic scoring system as a method for the prognosis of embryo implantation. J Assist Reprod Genet 2002;19(3):99-102.
44. Schild RL, Knobloch C, Dorn C, Fimmers R, van der Ven H, Hansmann M. Endometrial receptivity in an in vitro fertilization

program as assessed by spiral artery blood flow, endometrial thickness, endometrial volume, and uterine artery blood flow. Fertil Steril 2001;75(2):361-66.
45. Ardaens Y, Gougeon A, Lefebvre C, Thomas P, Lerov M, Lerov JL, Dewailly D. Contribution of ovarian and uterine color Doppler in medically assisted reproduction techniques (ART). Gynecol Obstet Fertil 2002;30(9):663-72.
46. Chien LW, Lee WS, Au HK, Tzeng CR. Assessment of changes in utero-ovarian arterial impedance during the peri-implantation period by Doppler sonography in women undergoing assisted reproduction. Ultrasound Obstet Gynecol 2004;23(5):496-500.
47. Kupesic S, Bekavac I, Bjelos D, Kurjak A. Assessment of endometrial receptivity by transvaginal color Doppler and three-dimensional power Doppler ultrasonography in patients undergoing in vitro fertilization procedures. J Ultrasound Med 2001;20(2):125-34.
48. Ng EHY, Chan CCW, Tang OS, Yeung WSB, Ho PC. Comparison of endometrial and subendometrial blood flow measured by three-dimensional power Doppler ultrasound between stimulated and natural cycles in the same patients. Hum Reprod 2004;19(10):2385-90.
49. Raine-Fenning NJ, Campbell BK, Kendall NR, Clewes JS, Johnxon IR. Quantifying the changes in endometrial vascularity throughout the normal menstrual cycle with three-dimensional power Doppler angiography. Hum Reprod 2004;19(2):330-38.
50. Yokota A, Nakai A, Oya A, Koshino T, Araki T. Changes in uterine and ovarian arterial impedance during the periovulatory period in conception and nonconception cycles. J Obstet Gynaecol Res 2000;26(6):435-40.
51. Kupesic S. Three-dimensional ultrasonographic uterine vascularization and embryo implantation. J Gynecol Obstet Biol Reprod (Paris) 2004;33(1 Pt 2):S18-20.
52. Buckett WM, Chian RC, Tan SL. Human chorionic gonadotropin for in vitro oocytes maturation: Does it improve the endometrium or implantation? J Reprod Med 2004;49(2):93-98.
53. Carbillon L, Perrot N, Uzan M, Uzan S. Doppler ultrasonography and implantation: A critical review. Fetal Diagn Ther 2001;16(6): 327-32.
54. Alcazar JL, Garcia-Manero M, Galvan R. Three-dimensional sonographic morphologic assessment of adnexal masses: A reproducibility study. J Ultrasound Med 2007;26 (8):1007-11.
55. Alcazar JL, Merce LT, Garcia-Manero M. Three-dimensional power Doppler vascular sampling: A new method for predicting ovarian cancer in vascularized complex adnexal masses. J Ultrasound Med 2005;24(5):689-96.
56. Poon CI, Zimmern PE. Role of three-dimensional ultrasound in assessment of women undergoing urethral bulking agent therapy. Curr Opin Obstet Gynecol 2004;16(5):411-17.
57. Dietz HP, Wilson PD. The 'iris effect': How two-dimensional and three-dimensional ultrasound can help us understand anti-incontinence procedures. Ultrasound Obstet Gynecol 2004; 23(3):267-71.